

Dispersive detection of single microwave photons with quantum dots

Stephanie Matern,¹ Alberto Biella,^{1,2} Pasquale Scarlino,³ Iacopo Carusotto,^{1,2} and Gianluca Rastelli^{1,2}

¹*CNR – INO Pitaevskii BEC Center and Dipartimento di Fisica, Università di Trento, Trento, Italy*

²*INFN-TIFPA, Trento Institute for Fundamental Physics and Applications, Via Sommarive 14, I-38123 Trento, Italy*

³*Institute of Physics and Center for Quantum Science and Engineering,
Ecole Polytechnique Fédérale de Lausanne, CH-1015 Lausanne, Switzerland*

(Dated: November 25, 2025)

Within a circuit quantum electrodynamics architecture, we theoretically investigate the detection of a single propagating microwave photon traveling through a resonant microwave cavity dispersively interacting with a double quantum dot tunnel-coupled to a lead. Under suitable conditions, a single photon in the cavity can induce a measurable change in the electronic occupation of the charge states. We develop a quantum cascade approach that enables a time-resolved description of a single-photon wave packet impinging on the cavity. We make use of a simple model of charge detector to assess the efficiency of our photo-detection configuration as functions of key parameters such as coupling strength, tunneling rate, temperature, and photon resonance linewidth. We finally highlight a measurement-induced backaction effect on the cavity mode associated with the dispersive, non-absorptive detection process.

I. INTRODUCTION

Circuit quantum electrodynamics (circuit QED) [1–3] has progressed through remarkable advances in superconducting devices, which not only serve as qubits for quantum information processing but can also be used for manipulation of quantum microwave fields. Despite major advances in microwave engineering, quantum photonics in this spectral domain remains at a much earlier stage compared to its optical counterpart. For instance, detecting a single itinerant microwave photon remains challenging due to its low energy. This represents a critical gap, as single-photon detection is fundamental in quantum optics [4], playing a key role in correlation measurements [5, 6], linear optics quantum computing [7], and remote entanglement protocols [8].

Using Josephson junction circuits, single microwave-photon detectors based on absorption processes have been realized through various schemes. One approach exploits metastability, as in current-biased Josephson junctions [9–15] acting as switching detectors [16–19], in SQUID devices with a double-well potential [20, 21], or in Kerr Josephson parametric resonators [22]. Another approach relies on engineered dissipation, such as impedance-matched Λ systems in 1D waveguide circuit QED [23–26], inelastic tunneling of quasiparticles in voltage-biased superconducting junctions [27, 28], or four-wave mixing systems incorporating a strongly damped cavity mode [29–33]. Moreover, bolometers scheme have bee also applied [34–36]. Additionally, non-absorbing detection has been demonstrated in pulsed-mode operation using a controlled-phase gate between a superconducting qubit and a propagating photon [37, 38], or by reaching the strong dispersive regime [39].

New perspectives for single microwave photons detection are offered by the combination of circuit QED systems with quantum dots (QDs). These act as artificial atoms [40–42] interacting with microwave photons in superconducting circuits [43, 44]. The uniqueness of

these systems lies in the seamless integration of quantum-coherent nanoscale devices, where semiconducting quantum nanostructures can be combined with superconducting elements and interfaced with a microwave photonic system [45–55]. They provide a framework to study light-matter interactions in the regime of coherent, far-from-equilibrium single-electron transport [56–74]. In particular, the regime of strong light-matter coupling has been reached for both charge [75–79] and spin qubits [80–83].

Early experiments showed that the absorption of a single photon can induce photo-assisted single-electron tunneling events [84–87]. The basic photon detection scheme has been studied in a double quantum dot (DQD) resonantly coupled to a microwave cavity mode [88, 89]: Photon absorption promotes an electron from the DQD ground (bonding) state to an excited (antibonding) state, from which it can tunnel to the leads. In this way, for asymmetric tunneling between the DQD and the left and right contacts, a steady photon flux generates a continuous, detectable charge current through the DQD. The experimental realization of this basic scheme was reported in [90] and in following related experiments [91–94]: While a proof of principle of the process was demonstrated, the detection efficiency η , defined as the ratio of photocurrent to photon flux, remained modest. A far improved efficiency $\eta \sim 70\%$ was reported in a later experiment [95].

All these experiments were based on photocurrent detection through a DQD, but individual photon-absorption events remain challenging to detect using current-based schemes. Single-electron tunneling events typically generate very short current pulses with amplitudes several orders of magnitude below the noise floor of available electronic instrumentation [96]. To overcome this limitation and enable detection of single-photon absorption events, an alternative approach was explored in [97], where charge-state switching in DQDs, triggered by a single absorbed photon, is monitored in real time using

a highly sensitive, fast charge sensor capacitively coupled to the dots. Although promising as strategy, the efficiency reported in this work remained as small as a few percent. Achieving a continuous mode single-photon microwave detection continues therefore to represent a significant open challenge in the field.

In this work, we analyze a minimal setup for achieving dispersive single-microwave-photon detection. The scheme leverages the experimental feasibility of monitoring the charge states in real time. The basic idea is illustrated in Fig. 1, providing a qualitative picture as described below. The effective model reduces to a single-electron level laterally tunnel-coupled to a lead (corresponding to the bonding charge state of the DQD, see Section A). Assuming an initial state in which the electronic level is well below the lead's chemical potential, the electronic state is fully occupied. When the photon enters the cavity, it induces a positive energy shift of the electronic state. If this shift is large enough, the electronic level moves above the chemical potential, allowing the electron to tunnel out to the lead. Once the photon leaves the cavity, the electronic state returns to its initial energy value, and it gets refilled by an electron tunneling in from the lead. Although this simplified picture strictly holds only at vanishing temperature, it motivates a detailed analysis of the system dynamics at finite temperature, to explore the parameter ranges (temperature, interaction strength, etc.) and assess its actual promise as photon detector.

The paper is structured as follows. In Section II we describe the effective model, formed by a single electron level tunnel-coupled to a macroscopic lead and dispersively interacting with a resonant mode of a microwave cavity. The full quantum dynamics of the system is governed by a Lindblad-like master equation. To model the dynamics of a single-photon wavepacket traveling towards the cavity, we use the quantum cascade approach. For the electron tunneling to the lead, we derive the corresponding dissipative superoperator in presence of the dispersive interaction with the microwave mode. In Section III, we present the results for the quantum dynamics of the system in the single-photon regime, explaining the behavior of the cavity and electron occupations as functions of the relevant parameters and highlighting a measurement-induced backaction effect on the cavity photon occupation. In Section IV, we analyze the detection efficiency based on a simple phenomenological model for the charge detector. In Section V, we critically discuss the challenges and experimental feasibility of our proposal. Finally, we draw our conclusions in Section VI.

II. THEORETICAL MODEL

The dispersive interaction between the DQD and the cavity mode reads

$$\hat{H}_{\text{dis}} = \omega_c \hat{n}_c + \epsilon \hat{n}_{\text{QD}} + \epsilon' \hat{n}'_{\text{QD}} + \lambda \hat{n}_c (\hat{n}'_{\text{QD}} - \hat{n}_{\text{QD}}), \quad (1)$$

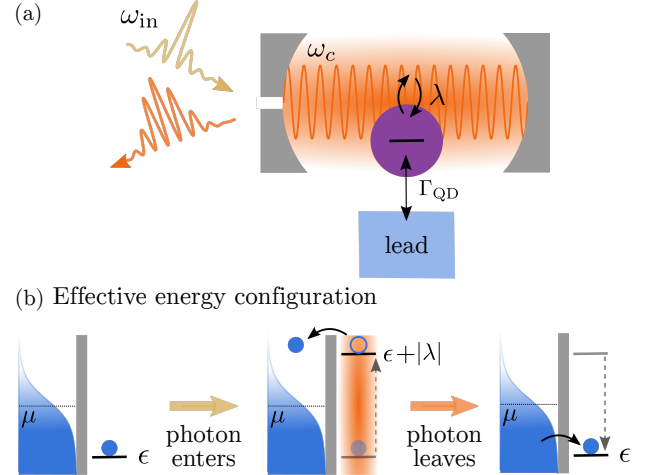


FIG. 1. (a) The system consists of an incoming microwave photon pulse with frequency ω_{in} , which is temporarily stored in a cavity (detection mode with frequency ω_c). The cavity is dispersively coupled (coupling strength λ) to a single electron state, from which an electron can tunnel to and from a single lead at temperature T and chemical potential μ with rate Γ_{QD} . (b) Concept of the dispersive measurement by monitoring the electron occupation. Initially, the energy of the electronic state is $\epsilon < \mu$, so this is almost fully occupied (in the low-temperature limit, see main text). When a photon enters the cavity, the energy of the electronic state shifts $\epsilon \rightarrow \epsilon + |\lambda|$, and the electron can tunnel out into the lead. The system charge occupation is monitored through a charge detector (not shown in the figure). Here we assumed the dispersive coupling $\lambda < 0$ (see main text). The single electron level corresponds to the bonding level of the DQD whereas the antibonding level (not shown) always remains empty, see Fig. 5 in Appendix A.

with the energy ϵ, ϵ' of the bonding and the antibonding levels respectively, ω_c is the frequency of the cavity mode and dispersive interaction strength λ . Hereafter we denote the resonant mode coupled to the DQD as the detection mode. The number operators read $\hat{n}_{\text{QD}} = \hat{d}^\dagger \hat{d}$ ($\hat{n}'_{\text{QD}} = \hat{d}^\dagger \hat{d}'$) and $\hat{n}_c = \hat{b}^\dagger \hat{b}$ in terms of the creation and annihilation operators of the electron levels (fermionic operators) and the detection mode (bosonic operators). We set $\hbar = k_B = 1$ throughout the paper.

A derivation of the effective dispersive Hamiltonian of Eq. (1) from the full Rabi model, a DQD coupled to a single microwave mode, is given in Section A (see also Refs. [98–100]). There, we also show that in a suitable parameter regime the antibonding state is irrelevant as its occupation remains unaffected by the photon occupation in the cavity (see Fig. 5). Then we can study the effective system composed by a single electronic level (the bonding state of the DQD) whose energy depends on the cavity photon occupation described by the following Hamiltonian

$$\hat{H}_S = \omega_c \hat{n}_c + \epsilon \hat{n}_{\text{QD}} - \lambda \hat{n}_c \hat{n}_{\text{QD}}. \quad (2)$$

Hereafter, we refer to the bonding state of the DQD as

the effective ‘QD single-electron level’ throughout the paper. Moreover, for definiteness, we choose for the rest of the discussion the bonding to antibonding energy transition in the DQD on the red side of the cavity mode, $\Omega < \omega_c$, so that we have $\lambda < 0$. As a consequence, we consider the initial level of the bonding state ϵ (with no photon in the cavity) to be below the chemical potential ($\epsilon < \mu$) of the lead to which the DQD is laterally tunnel-coupled. Alternatively, one can assume $\lambda > 0$ and set $\epsilon > \mu$ for the initial state of the bonding state, see Fig. 5.

A. Tunneling dynamics with dispersive interaction

As mentioned above, the single QD level is tunnel-coupled to the lateral lead which is modeled as a free Fermi gas. Then, starting from the Bloch-Redfield-Wangness equation [101] containing the tunneling between the lead and the single QD level dispersively coupled to the detection mode, we trace out the degrees of freedom of the lead. We thus derive the following superoperator, valid in the single-photon regime

$$\begin{aligned} \frac{\mathcal{L}_{\text{QD}}[\hat{\rho}]}{\Gamma_{\text{QD}}} = & -f(\epsilon) \left[\left\{ \hat{\Pi}_0 \hat{d} \hat{d}^\dagger; \hat{\rho} \right\} - 2\hat{\Pi}_0 \hat{d}^\dagger \hat{\rho} \hat{d} \hat{\Pi}_0 \right] \\ & - f(\epsilon + |\lambda|) \left[\left\{ \hat{\Pi}_1 \hat{d} \hat{d}^\dagger; \hat{\rho} \right\} - 2\hat{\Pi}_1 \hat{d}^\dagger \hat{\rho} \hat{d} \hat{\Pi}_1 \right] \\ & - (1 - f(\epsilon)) \left[\left\{ \hat{\Pi}_0 \hat{d}^\dagger \hat{d}; \hat{\rho} \right\} - 2\hat{\Pi}_0 \hat{d} \hat{\rho} \hat{d}^\dagger \hat{\Pi}_0 \right] \\ & - (1 - f(\epsilon + |\lambda|)) \left[\left\{ \hat{\Pi}_1 \hat{d}^\dagger \hat{d}; \hat{\rho} \right\} - 2\hat{\Pi}_1 \hat{d} \hat{\rho} \hat{d}^\dagger \hat{\Pi}_1 \right] \\ & + [f(\epsilon) + f(\epsilon + |\lambda|)] \left(\hat{\Pi}_0 \hat{d}^\dagger \hat{\rho} \hat{d} \hat{\Pi}_1 + \hat{\Pi}_1 \hat{d}^\dagger \hat{\rho} \hat{d} \hat{\Pi}_0 \right) \\ & + [2 - f(\epsilon) - f(\epsilon + |\lambda|)] \left(\hat{\Pi}_0 \hat{d} \hat{\rho} \hat{d}^\dagger \hat{\Pi}_1 + \hat{\Pi}_1 \hat{d} \hat{\rho} \hat{d}^\dagger \hat{\Pi}_0 \right). \end{aligned} \quad (3)$$

Here, Γ_{QD} is the tunneling rate of the QD describing the electron exchange with the lead and the Fermi function $f(\epsilon) = \{1 + \exp[(\epsilon - \mu)/T]\}^{-1}$ with temperature T and chemical potential μ of the lead. The two projectors $\hat{\Pi}_0 = 1 - \hat{n}_c$ and $\hat{\Pi}_1 = \hat{n}_c$ define the projection onto the Fock states of the detection mode with zero or one photon occupation. The first four terms of Eq. (3) correspond to a Lindblad dissipator conditioned on photon occupation of the detection mode. The Fermi function appearing in the electron tunneling rate is adjusted accordingly, depending on the photon occupation. The remaining terms capture the coherences between the 0 and 1 photon subspace. In the limit $|\lambda| \rightarrow 0$, one recovers the Lindblad operator for a single QD level coupled to a Fermi reservoir. The full derivation of Eq. (3) is given in Section B.

In deriving Eq. (3), we assume that the QD electronic state is weakly tunnel-coupled to the lateral lead, so that the interaction can be treated perturbatively to first order (i.e., in the sequential tunneling regime). Higher-order (cotunneling) terms, corresponding to quantum fluctuations of electron tunneling and leading to renormalization effects, are negligible. In our setup, when a

photon enters the cavity, the QD is in a metastable state, assuming the single QD level predominantly occupied. An electron can then tunnel out with the simple transition rate $\sim \Gamma_{\text{QD}}$ even in the low-temperature limit. We argue that this perturbative Markovian approach where cotunneling and non-Markovian corrections are negligible is valid under the conditions: (i) The transparency of the barrier is low, i.e., the tunnel resistance is much larger than quantum resistance. (ii) The electron conducting bandwidth of the contact is much larger than Γ_{QD} , (iii) The linewidth of the single electron level is smaller than the distance from the chemical potential, $\Gamma_{\text{QD}} \ll |\epsilon - \mu|$, which implies that statistical, fermionic correlations are irrelevant.

B. Quantum cascade model

In order to describe the incoming photon entering the detection cavity, we use the quantum cascade approach [102, 103]. It allows for a time-resolved description of a single-photon wavepacket impinging on the cavity and captures both the coherent evolution and the interaction-induced modifications of the quantum state during the scattering process. This approach is based on a microscopic model involving an ancillary cavity mode (source mode) and a detection mode, both coupled to a chiral transmission line at zero temperature.

The source mode has frequency ω_{in} and bosonic operators, annihilation and creation, $(\hat{a}, \hat{a}^\dagger)$, with occupation number $\hat{n}_{\text{in}} = \hat{a}^\dagger \hat{a}$, and we set

$$\hat{H}_{\text{in}} = \omega_{\text{in}} \hat{n}_{\text{in}}. \quad (4)$$

The decay of this source mode into the transmission line provides the incoming photon that hits the detector and sets its spectral linewidth.

After tracing out the transmission line, one obtains an effective dissipative, nonreciprocal interaction between the detection and source mode. The corresponding superoperator involving the two modes’ operators reads [102, 103]

$$\begin{aligned} \mathcal{L}_{\text{cas}}[\hat{\rho}] = & -\gamma_{\text{in}} \left[\left\{ \hat{a}^\dagger \hat{a}; \hat{\rho} \right\} - 2\hat{a} \hat{\rho} \hat{a}^\dagger \right] \\ & - \gamma_c \left[\left\{ \hat{b}^\dagger \hat{b}; \hat{\rho} \right\} - 2\hat{b} \hat{\rho} \hat{b}^\dagger \right] \\ & - 2\sqrt{\gamma_{\text{in}} \gamma_c} \left[\hat{b}^\dagger \hat{a} \hat{\rho} + \hat{\rho} \hat{a}^\dagger \hat{b} - \hat{b} \hat{\rho} \hat{a}^\dagger - \hat{a} \hat{\rho} \hat{b}^\dagger \right], \end{aligned} \quad (5)$$

where $\{\cdot; \cdot\}$ denotes the anticommutator. The parameter γ_{in} represents the bandwidth of the source whereas γ_c corresponds the photon losses of the detection mode. Although the derivation of Eq. (5) was given in [102] and in [103], for completeness, we provide another, independent derivation in Section C starting from a Bloch-Redfield-Wangness equation [101] containing the coupling between the two modes and the chiral line. Note that it is also possible to rewrite the dissipative interaction of Eq. (5) in Lindblad form using jump operators given by a linear

combination of the bosonic operators and introducing an effective coherent coupling between the source and the detection mode [102].

C. Equation for the density matrix

Combining the dissipators for electronic and photonic part, the full time evolution of the composite system is governed by the master equation for the density matrix

$$\frac{d\hat{\rho}}{dt} = -i \left[H_S + \hat{H}_{\text{in}}; \hat{\rho} \right] + \mathcal{L}_{\text{QD}} [\hat{\rho}] + \mathcal{L}_{\text{cas}} [\hat{\rho}], \quad (6)$$

where $[\cdot, \cdot]$ denotes the commutator. Then, Eq. (6) generates a set of coupled and closed linear equations for the matrix elements (see Section D), which can be solved exactly.

III. DISPERSIVE MEASUREMENT AND BACKACTION

The goal is to detect a single photon by monitoring the alteration of the QD occupation in response to the presence of the photon in the cavity. The dispersive nature of the coupling between the detection cavity mode and the QD ensures that the photon is not destroyed by the measurement process.

Fixing the chemical potential of the lead $\mu = 0$, we assume the system is initialized as follows. The QD level is set to $\epsilon = -|\lambda|/2$ and the QD is in its stationary state with occupation probability $p^{(1)}(t=0) = p_s^{(1)}$ and $p^{(0)}(t=0) = p_s^{(0)}$. The subscript s denotes the stationary state which is given by $p_s^{(0)} = 1 - f(\epsilon)$ and $p_s^{(1)} = f(\epsilon)$ for a given temperature T of the lead. In the limit $T \rightarrow 0$, the QD is fully occupied and $p_s^{(1)} = 1$. The detection mode with frequency ω_c is empty, $\langle \hat{n}_c(t=0) \rangle = 0$, whereas the source mode is occupied, $\langle \hat{n}_{\text{in}}(t=0) \rangle = 1$. The source mode is on resonance with the cavity mode when its frequency ω_{in} is set to $\omega_c + |\lambda|$, as the QD is initially occupied. If now the incoming photon occupies the detection mode, the QD level shifts $\epsilon \rightarrow \epsilon + |\lambda| = |\lambda|/2$. With an energy above the Fermi level of the lead, the electron on the dot can leave on a time scale set by $1/\Gamma_{\text{QD}}$.

A. Time evolution

The time evolution of the system can be obtained by solving Eq. (6). The transient dynamics of the relevant observables, i.e., the QD probabilities $p^{(1)}(t)$ ($p^{(0)}(t) = 1 - p^{(1)}(t)$), the occupation of the detection mode $\langle \hat{n}_c(t) \rangle$ and source mode $\langle \hat{n}_{\text{in}}(t) \rangle$ are shown in Fig. 2 for the initial conditions discussed above.

The average photon occupation of the source mode $\langle \hat{n}_{\text{in}}(t) \rangle$ decays exponentially on a time scale $\sim 1/\gamma_{\text{in}}$. Due to the unidirectional interaction between source and

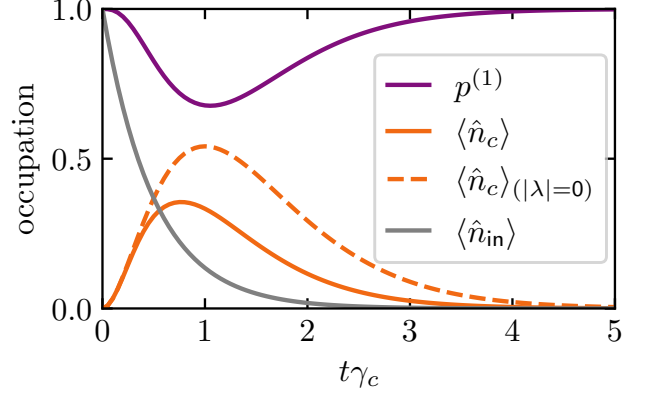


FIG. 2. Example of time evolution of the QD occupation $p^{(1)}$ (purple), the source mode $\langle \hat{n}_{\text{in}} \rangle$ (gray), and the detection mode $\langle \hat{n}_c \rangle$ (solid orange line) for $\omega_{\text{in}} = \omega_c + |\lambda|$, $\Gamma_{\text{QD}} = 4\gamma_c$, $\epsilon = -|\lambda|/2$, $\gamma_{\text{in}} = \gamma_c = 0.01\omega_c$, $\gamma_c = 0.1|\lambda|$, and $T = 0.01|\lambda|$. To show the effect of the backaction due to the dispersive interaction, which always leads to a decrease of $\langle \hat{n}_c \rangle$, the detection mode occupation for $\lambda = 0$, $\langle \hat{n}_c \rangle_{(\lambda=0)}$, is plotted for comparison (orange dashed line).

detection mode, $\langle \hat{n}_{\text{in}}(t) \rangle$ is independent of all other system parameters

$$\langle \hat{n}_{\text{in}}(t) \rangle = e^{-2\gamma_{\text{in}}t}. \quad (7)$$

The evolution of the average occupation of the detection mode, in the limit $|\lambda| = 0$, when its evolution fully decouples from the QD, is given by

$$\langle \hat{n}_c(t) \rangle_{(|\lambda|=0)} = \frac{8\gamma_{\text{in}}\gamma_c}{(\gamma_{\text{in}} - \gamma_c)^2 + \Delta\omega^2} e^{-2(\gamma_{\text{in}} + \gamma_c)t} \{ \cosh[(\gamma_{\text{in}} - \gamma_c)t] - \cos(\Delta\omega t) \}, \quad (8)$$

with the detuning $\Delta\omega = \omega_{\text{in}} - \omega_c$. The initially empty cavity becomes populated with increasing time. The maximal occupation has an upper bound $n_{\text{max}}^{(0)} = 4/e^2$ for $\Delta\omega = 0$ and $\gamma_{\text{in}} = \gamma_c$. Then, for long times $t \gg 1/\gamma_c$, $\langle \hat{n}_c(t) \rangle$ decays exponentially.

In presence of the dispersive interaction with the QD $|\lambda| \neq 0$, $\langle \hat{n}_c(t) \rangle$ has a similar, non-monotonic behavior. The full evolution depends now on all system parameters. Further analytical expressions are given in Section D. The crucial general feature is that, overall, the probability of the detection mode occupation is suppressed in presence of the dispersive coupling with the QD. We will analyze this measurement-induced backaction in the next section.

The evolution of the QD occupation is correlated with the one of the detection mode with $p^{(0)}(t) = 1 - p^{(1)}(t)$ behaving similarly to $\langle \hat{n}_c(t) \rangle$. The electron in the QD level can tunnel out when the photon is in the cavity. Once the photon left the cavity, the state of QD level relaxes to the initial state which, in the limit of low temperature $T \ll |\lambda|$, corresponds to the occupied state, as shown in Fig. 2.

B. Backaction of the dispersive measurement

As shown in Fig. 2, we observe a backaction effect due to the dispersive coupling with the QD: The photon occupation of the detection mode is significantly reduced compared to the uncoupled case. This can be explained as a suppression of the coherence in the transfer of the photon into the detection cavity.

To analyze this result in detail, it is useful to analyze the behavior of the density matrix components which we define as

$$\rho_{n_s n_d, \tilde{n}_s \tilde{n}_d}^{c\tilde{c}} = \langle n_s, n_d, c | \hat{\rho} | \tilde{n}_s, \tilde{n}_d, \tilde{c} \rangle. \quad (9)$$

Here, $c, \tilde{c} = 0, 1$ denote the occupation of the QD, $n_s, \tilde{n}_s = 0, 1$ is the occupation of the source mode and $n_d, \tilde{n}_d = 0, 1$ the number of photons in the detection mode. The equations of motion for each density matrix component are given in Section D.

The initially occupied source mode $\rho_{10,10}^{c\tilde{c}}$ acts as source term in the equations of motion for $\rho_{10,01}^{c\tilde{c}}$ (off-diagonal in the photon subspace). The latter is itself coupled to the occupation of the detection mode $\rho_{01,01}^{c\tilde{c}}$, such that we end up with sequential coupled equations for the components,

$$\rho_{10,10}^{c\tilde{c}} \longrightarrow \rho_{10,01}^{c\tilde{c}} \longrightarrow \rho_{01,01}^{c\tilde{c}}. \quad (10)$$

A reduction of $\rho_{10,01}^{c\tilde{c}}$ translates into a decrease of $\rho_{01,01}^{c\tilde{c}}$, therefore reducing the probability of absorption in the detection mode. Thus, to explain the backaction, we focus hereafter on the behavior of the density matrix components $\rho_{10,01}^{00}$ and $\rho_{10,01}^{11}$ which are diagonal in charge, and off-diagonal in the photon subspace. They capture the coherence of the photonic part of the system playing a crucial role for the photon injection.

To qualitatively capture the main features, we consider the limit of $T \rightarrow 0$, where

$$\begin{aligned} \dot{\rho}_{10,01}^{00} &= -2\sqrt{\gamma_{\text{in}}\gamma_c}\rho_{10,10}^{00} + \frac{\Gamma_{\text{QD}}}{2}\rho_{10,01}^{11} \\ &\quad - \left[\frac{\Gamma_{\text{QD}}}{2} + \gamma_{\text{in}} + \gamma_c + i\Delta\omega \right] \rho_{10,01}^{00}, \\ \dot{\rho}_{10,01}^{11} &= -2\sqrt{\gamma_{\text{in}}\gamma_c}\rho_{10,10}^{11} + \frac{\Gamma_{\text{QD}}}{2}\rho_{10,01}^{00} \\ &\quad - \left[\frac{\Gamma_{\text{QD}}}{2} + \gamma_{\text{in}} + \gamma_c + i(\Delta\omega - |\lambda|) \right] \rho_{10,01}^{11}. \end{aligned} \quad (11)$$

Setting $|\lambda| = 0$, the evolution of the QD and photon modes decouples. In this case Eq. (11) admit factorized solutions and one can consider the single equation of motion for the photonic off-diagonal component $\rho_{10,01} = \rho_{10,01}^{00} + \rho_{10,01}^{11}$ (fully independent of Γ_{QD}). Increasing the detuning $\Delta\omega$ leads to a decrease of $\rho_{10,01}$.

For $|\lambda| \neq 0$, in particular setting $\Delta\omega = |\lambda|$ in Eq. (11), we see that the evolution of $\rho_{10,01}^{11}$ is independent of $|\lambda|$, since the resonance condition between the detection mode and the incoming photon is fulfilled when the dot is occupied. In contrast, for the $\rho_{10,01}^{00}$ with $|\lambda| = \Delta\omega$, the

dispersive coupling acts similarly to a detuning since the frequency of the detection mode is no longer on resonance with the incoming photon when the dot is empty. Consequently, increasing $|\lambda|$ has, qualitatively speaking, the same effect of reducing the cavity absorption probability as increasing the $\Delta\omega$ in the uncoupled case. This effect is significant when photon induced detuning is comparable to the linewidth $|\lambda| \gtrsim \gamma_c$.

Another important observation is that the detection mode occupation does not vanish in the limit $|\lambda| \rightarrow \infty$, since there is always a finite probability that the electron does not tunnel to the lead for finite values of Γ_{QD} , (i.e., $\rho_{10,01}^{11}$ is independent of $|\lambda|$) and, in this case, the photon frequency remains unperturbed. In fact, when the tunneling process is slow (i.e., the tunneling rate is low $\Gamma_{\text{QD}} \ll \gamma_c$), the QD single-level does not have enough time to transfer its electron to the lead and therefore remains occupied even if the photon stays inside the cavity. In this case, the photon cannot be detected. Conversely, when tunneling is fast $\Gamma_{\text{QD}} \gg \gamma_c$, the electron quickly jumps to the lead, shifting the cavity mode out of resonance. This possibility of rapid measurement significantly destroys coherence for $|\lambda| \gg \gamma_c$, lowering the probability that a photon will enter the cavity.

All the qualitative features discussed so far for $\langle \hat{n}_c(t) \rangle$ are consistent with the full solution which is stated in Eq. (D9).

C. Maximum photon occupation and QD depletion

As the incoming photon only occupies the detection mode for a finite amount of time, the dispersive measurement relies on a transient effect. To summarize the dependence on various parameters, in the following we show: (i) The maximal detection mode occupation $n_{\text{max}} = \max_t \langle \hat{n}_c(t) \rangle$, and (ii) the maximal change in QD occupation over all times t , $\Delta p_{\text{max}} = \max_t [p^{(0)}(t) - p^{(0)}(t=0)]$, see Fig. 3. In the following, we analyze for these two quantities the interplay between the different parameters, namely the detuning $\Delta\omega$, the QD rate Γ_{QD} , and the bandwidth of the incoming photon pulse γ_{in} , for given ranges of the dispersive coupling $|\lambda|$ and the temperature T .

1. Dependence on the detuning $\Delta\omega$

The left panel in Fig. 3(a) illustrates the matching condition needed to maximize the occupation of the detection photon mode for an initially occupied QD at $T \ll |\lambda|$. As expected, for a given $|\lambda|$ this resonance occurs at $\Delta\omega = |\lambda|$.

As a function of $|\lambda|$, the general trend is, as mentioned before, that the height n_{max} of the resonance peak decreases for increasing $|\lambda|$. The reduction predominately depends on how $|\lambda|$ compares to γ_c : for small enough $|\lambda|$ the shift of the cavity's resonance frequency between ω_c

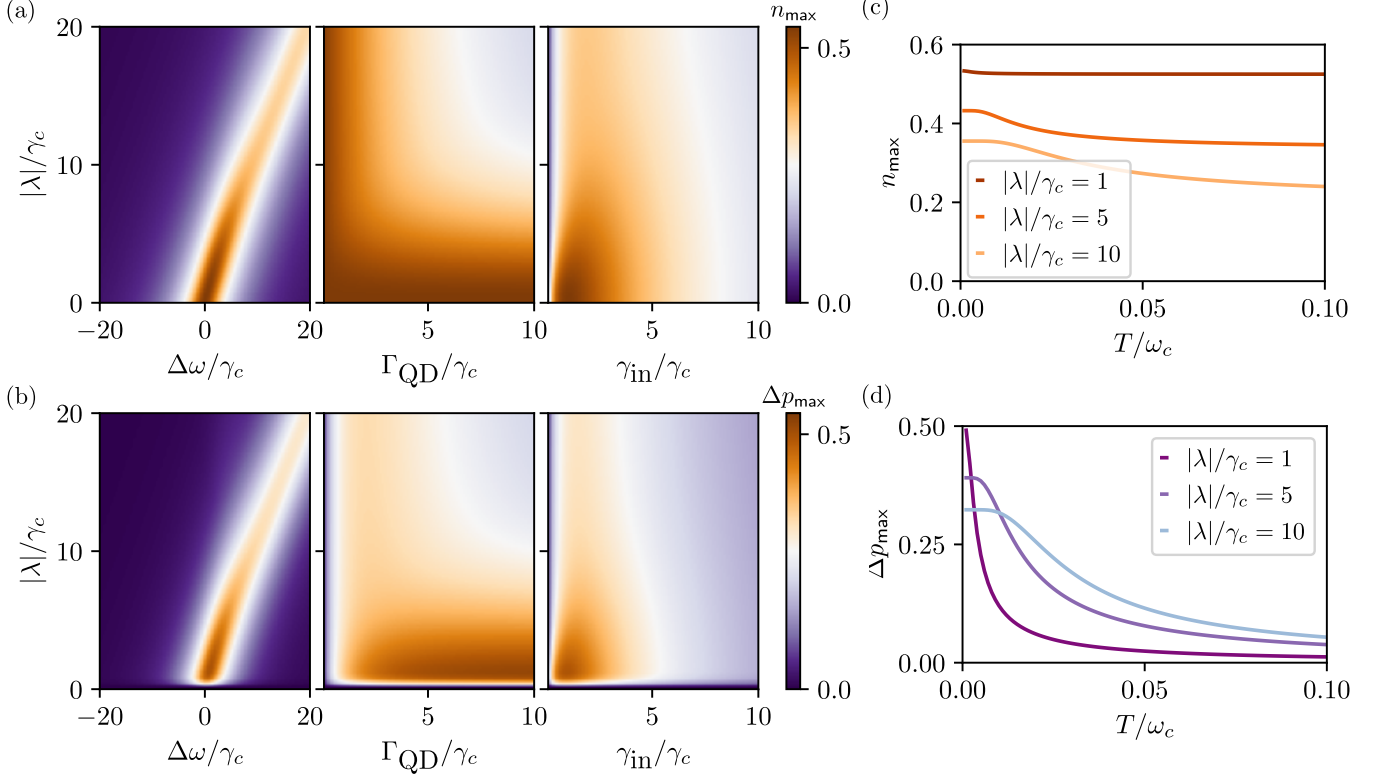


FIG. 3. (a) n_{\max} as function of $|\lambda|$ and system parameters $\Delta\omega$ (left), Γ_{QD} (middle), and γ_{in} (right). (b) Δp_{\max} as a function of the same parameters as in (a). (c) T dependence of n_{\max} and (d) Δp_{\max} along cuts of constant $|\lambda|$. Constant parameters in all subfigures are set to $T = 0.1\gamma_c$, $\epsilon = -|\lambda|/2$ and $\gamma_c = \gamma_{\text{in}} = 0.01\omega_c$, $\Gamma_{\text{QD}} = 4\gamma_c$, $\Delta\omega = |\lambda|$.

and $\omega_c + |\lambda|$ due to coupling to the QD is within the line width of detection mode. As $|\lambda|$ increases to $|\lambda| \gg \gamma_c$, the dispersive frequency shift becomes larger than the line width and the coherence between the photon modes is suppressed as explained in the previous section.

The maximal detection mode occupation is bounded from above by $n_{\max}^{(0)}$. The lower bound is attained in the limit $|\lambda| \rightarrow \infty$, remaining strictly positive for finite value of the QD lifetime $1/\Gamma_{\text{QD}}$. As explained before, for $|\lambda| \rightarrow \infty$, the photon occupation does not vanish due to the finite probability that the QD remains occupied without inducing a frequency shift of the cavity mode.

Concerning the QD, shown in the left panel of Fig. 3(b), Δp_{\max} mirrors the behavior of n_{\max} . The strong correspondence shows that by monitoring the QD depletion we have access to the occupation of the detection mode. Notice that, for $|\lambda| \ll T$, thermal fluctuations of the QD smear out Δp_{\max} (see the discussion in sec. III C 4).

2. Dependence on the tunneling rate Γ_{QD}

The central panel of Fig. 3(a) shows n_{\max} for varying Γ_{QD} and $|\lambda|$, assuming the resonant condition $\Delta\omega = |\lambda|$.

Here, we observe a first regime in which n_{\max} re-

mains almost unperturbed by the dispersive measurement, $n_{\max} \approx n_{\max}^{(0)}$. This occurs for $|\lambda| \ll \gamma_c$, when n_{\max} is almost unaffected by Γ_{QD} . In this case, the dispersive frequency shift of the detection mode induced by the QD charge depletion is smaller than the photon linewidth. As discussed in the previous section, the cavity occupation is thus unaffected by the charge dynamics and does not depend on Γ_{QD} .

The second regime occurs for $|\lambda| \gg \gamma_c$ where one recovers the expected behavior discussed earlier: For $\Gamma_{\text{QD}} < \gamma_c$ the tunneling process is slow, the QD's occupation does not have enough time to switch within the photon lifetime in the cavity, resulting in an effective non-measurement. Thus the photon occupation remains almost unaffected by the dispersive interaction. As Γ_{QD} increases, $\Gamma_{\text{QD}} \gg \gamma_c$, the photon occupation diminishes due to the QD measurement.

The central panel of Fig. 3(b) shows Δp_{\max} as a function of Γ_{QD} and $|\lambda|$, assuming the resonant condition $\Delta\omega = |\lambda|$. The effect of the finite temperature is again visible at small value of coupling $|\lambda| < T$, where thermal fluctuations of the QD occupation are comparable to the QD depletion caused by the photon cavity occupation (see the discussion in Sec. III C 4). Excluding this region affected by temperature, the behavior of Δp_{\max} is correlated with that of n_{\max} shown in the central panel

of Fig. 3(a) and we summarize it in two distinct regimes.

In the first regime, when $|\lambda| > \gamma_c$, the dispersive interaction can affect the photon occupation. However, at slow tunneling rates, $\Gamma_{\text{QD}} < \gamma_c$, the charge switching is slow, and the charge depletion Δp_{max} remains small: the QD occupation has a low probability of switching, i.e., $\Delta p_{\text{max}} = 0$ for $\Gamma_{\text{QD}} \rightarrow 0$, and the photon entering the cavity is almost unperturbed. At fast tunneling rates, $\Gamma_{\text{QD}} > \gamma_c$, the charge can tunnel readily, allowing the measurement to occur. This induces backaction, which reduces the photon occupation and, in turn, decreases the probability that the electronic level is shifted to allow the electron to tunnel. The interplay of these two effects leads to a nonmonotonic behavior of Δp_{max} as a function of Γ_{QD} when $|\lambda| > \gamma_c$.

In the second regime, when $|\lambda| < \gamma_c$, the dispersive interaction cannot affect the photon occupation, as visible in the central panel of Fig. 3(a). At the same time, at sufficiently fast tunneling rates, $\Gamma_{\text{QD}} > \gamma_c$, one may argue that the charge can tunnel readily, allowing the measurement to occur, as visible in the central panel of Fig. 3(b). In other words, in this region, we may expect to have both: (i) The probability of the photon entering the cavity remains unperturbed by the coupling to the QD (i.e., no backaction) (ii) High internal efficiency, i.e., the probability to detect the photon assuming that it is in the cavity is high. Note however that in this region, defined by $T < |\lambda| < \gamma_c < \Gamma_{\text{QD}}$, which a priori should be the optimal regime, our approach can unfortunately provide only a qualitative picture, since $|\epsilon - \mu| = |\lambda|/2$ is comparable to or smaller than Γ_{QD} and non-Markovian effects can become significant (see discussion in Sec. II A).

3. Dependence on the bandwidth γ_{in}

The right panels of Fig. 3(a) and (b) show the dependence of n_{max} and Δp_{max} on γ_{in} .

Regarding the cavity, n_{max} reaches its maximum around $\gamma_{\text{in}} = \gamma_c$, as discussed earlier. Decreasing or increasing γ_{in} leads to smaller values of n_{max} . For larger values of the dispersive interaction $|\lambda| > 0$, the photon occupation as a function of γ_{in} exhibits the same qualitative nonmonotonic behavior; however, the peak value of n_{max} is suppressed as $|\lambda|$ increases, as discussed above.

Overall, the behavior of Δp_{max} shown in the right panel of Fig. 3(b) reflects that of n_{max} in most of its features. As a main exception, a marked difference is again visible in the narrow region $|\lambda| < T$ where, as mentioned above, the finite temperature washes out the effect of the photon.

4. Dependence on the temperature T

The T dependence of n_{max} and Δp_{max} are shown in Fig. 3(c) and (d). First, we observe that, for $|\lambda| \leq \gamma_c$, effect of the QD on the photon is negligible and n_{max}

results to be almost independent of T . For larger values of $|\lambda| > \gamma_c$, instead, the backaction of the QD becomes significant, reducing n_{max} at $T = 0$. As the temperature increases, for $T \gg |\lambda|$, the initial thermal equilibrium probabilities $p_s^{(0)}$ and $p_s^{(1)}$ saturate to 1/2, since we have fixed $|\epsilon - \mu| = |\lambda|/2$. On the one hand, such strong thermal fluctuations of the QD occupation lead to a random detuning of the cavity mode, resulting in a significant reduction of the photon occupation, see Fig. 3(c). On the other hand, the thermal broadening of the lead is large enough that the level shift due to a photon in the cavity has no effect on the fluctuating tunneling dynamics, which suppresses Δp_{max} , see Fig. 3(d).

IV. DETECTION EFFICIENCY

Charge detection to measure the QD population is routinely implemented in current experiments, for instance, via monitoring the impedance of quantum nanoconductors capacitively coupled to the measured QD. A discussion of this and other experimental issues is given in Section V. Here we provide quantitative estimates for the detection efficiency of our proposed scheme by using a phenomenological model of a charge detector.

This model is based on an additional two-level system coupled only to the QD, which gets excited when the QD population changes from full to empty. This process can be included in the master equation (6) by adding the dissipator

$$\frac{\mathcal{L}_{\text{det}}[\hat{\rho}]}{\gamma_{\text{det}}} = - \left[\left\{ \hat{\Pi}_0^{\text{QD}} \hat{\sigma}^- \hat{\sigma}^+; \hat{\rho} \right\} - 2 \hat{\Pi}_0^{\text{QD}} \hat{\sigma}^+ \hat{\rho} \hat{\sigma}^- \hat{\Pi}_0^{\text{QD}} \right], \quad (12)$$

where $\hat{\sigma}^+, \hat{\sigma}^-$ are the raising/lowering operators for the detector two-level system and γ_{det} denotes the charge detector rate. The operator $\hat{\Pi}_0^{\text{QD}} = 1 - \hat{n}_{\text{QD}}$ projects onto the unoccupied QD state, so to describe that the detector only clicks when the QD is empty. Adding this dissipator modeling the detector has no effect on the dynamics of the system of the QD and of the cavity mode. In order to estimate the detection efficiency, we consider that the QD is initially in the occupied state $p^{(1)}(t = 0) = 1$. This can be ensured by monitoring the QD's occupation, see Section V. At the same time, the detection two-level system is also initialized in its ground state.

At zero temperature $T = 0$, the long-time limit of the detector's occupation $\langle \hat{n}_{\text{det}} \rangle$ coincides with the efficiency of detecting the photon, as

$$\lim_{t \rightarrow \infty} \langle \hat{n}_{\text{det}}(t) \rangle < 1, \quad (13)$$

where $\hat{n}_{\text{det}} = \hat{\sigma}^+ \hat{\sigma}^-$. However, at finite T the QD occupation can change due to thermal fluctuations and consequently $\langle \hat{n}_{\text{det}} \rangle \rightarrow 1$ for $t \rightarrow \infty$, independently of the occupation of the detection mode. Indeed, even for the QD decoupled from the detection cavity mode, $\lambda = 0$, $\langle \hat{n}_{\text{det}}^{(|\lambda|=0)} \rangle \rightarrow 1$ for $t \rightarrow \infty$. Here, $\langle \hat{n}_{\text{det}}^{(|\lambda|=0)} \rangle$ denotes the detector's occupation arising from the thermal background

associated to the dark count rate, namely the electron tunneling rate from the occupied QD into the lead at finite temperature

$$p_{\text{dark}} = \Gamma_{\text{QD}} [1 - f(-|\lambda|/2)]. \quad (14)$$

For $T \ll |\lambda|$, p_{dark} is exponentially small.

For a proper detector, one requires a very low value of the dark counts in the typical lifetime of the photon in the cavity and, at the same time, a fast tunneling rate to detect the photon

$$p_{\text{dark}} \ll \gamma_c \ll \Gamma_{\text{QD}}. \quad (15)$$

In this limit, taking into account the thermal noise of the QD, we define

$$\Delta n_{\text{det}}(t) = \langle \hat{n}_{\text{det}}(t) \rangle - \langle \hat{n}_{\text{det}}^{(|\lambda|=0)}(t) \rangle, \quad (16)$$

with $\Delta n_{\text{det}} \rightarrow 0$ for $t \rightarrow \infty$. Moreover, for sufficiently low dark count rate (examples are shown in the dark curves in Fig. 4(a-b)), a time-scale separation can occur: The effect of thermal dark counts remains small, and the behavior of Δn_{det} is primarily determined by the behavior of the QD level occupation. In such a regime, $\Delta n_{\text{det}}(t)$ is (almost) constant for a time during which its value is directly related to the depletion of the QD level, and therefore correlated with the photon occupation. In this regime, we define the detector efficiency as

$$\eta = \max_t \Delta n_{\text{det}}(t). \quad (17)$$

In Fig. 4(a) and (b), we show the time evolution of $\Delta n_{\text{det}}(t)$ for the limiting cases of a slow detector with $\gamma_{\text{det}} \ll \Gamma_{\text{QD}}$, and a fast detector with $\gamma_{\text{det}} \gg \Gamma_{\text{QD}}$, for two temperature choices: $T = 0.01|\lambda|$ and $T = 0.25|\lambda|$.

In Fig. 4(a) we observe that $\Delta n_{\text{det}}(t)$ reaches a (quasi-) constant value for the selected temperature range. These values are reached almost immediately after the transient depletion of the QD level, and the probability $p^{(0)}(t)$ (plotted as filled areas in Fig. 4) returns to zero. For low dark count and when γ_{det} is the smallest rate, we obtain that the numerical value of η is in a very good agreement with the linear response quantity $\eta^* = \gamma_{\text{det}} \int_0^\infty dt \Delta p^0(t)$ [dotted lines in Fig. 4(a)].

In Fig. 4(b), for $\gamma_{\text{det}} = 100\Gamma_{\text{QD}}$, only in the low T limit the time scales remain well separated, the dark count rate is low and the (quasi-) plateau is visible. The dark counts associated with the thermal noise becomes relevant already for $T = 0.25|\lambda|$: Δn_{det} does not show a plateau but simply a nonmonotonic behaviour.

In Fig. 4(c) we plot the full time evolution $\langle \hat{n}_{\text{det}} \rangle$ (solid lines) compared to $\langle \hat{n}_{\text{det}}^{(|\lambda|=0)} \rangle$ (dashed lines) for $\gamma_{\text{det}} = 100\Gamma_{\text{QD}}$ for different temperatures. For high T , on the time scale $1/\gamma_c$, the well-defined plateau that defines η vanishes, as $\langle \hat{n}_{\text{det}}(t) \rangle \rightarrow 1$ rapidly due to the increasing thermal noise. For intermediate- and low- T , instead, the single photon yields a sharp increase up to the plateau and the dark counts are visible only at later times.

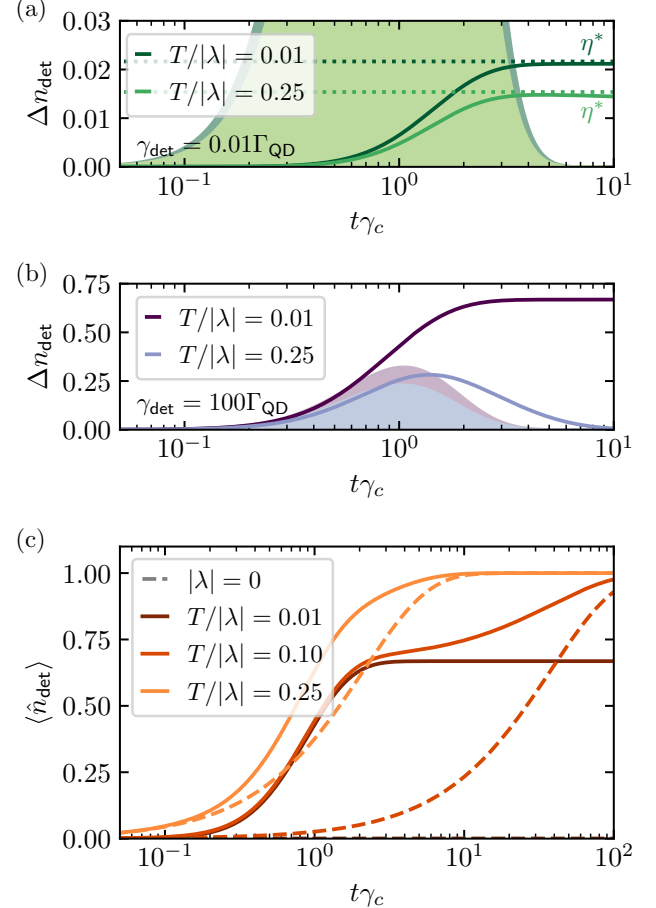


FIG. 4. Full time evolution of $\Delta n_{\text{det}}(t)$ for different temperatures, for (a) $\gamma_{\text{det}} = 0.01\Gamma_{\text{QD}}$ (solid lines) and (b) $\gamma_{\text{det}} = 100\Gamma_{\text{QD}}$ (solid lines). The evolution of $p^{(0)}(t)$ is also shown for comparison (filled areas) for the corresponding choice of T . In (a) the dotted lines correspond to η^* (see text). (c) Full time evolution $\langle \hat{n}_{\text{det}} \rangle$ (solid lines) and $\langle \hat{n}_{\text{det}}^{(|\lambda|=0)} \rangle$ (dashed lines) for different temperatures and for $\gamma_{\text{det}} = 100\Gamma_{\text{QD}}$. Notice that the curve $\langle \hat{n}_{\text{det}}^{(|\lambda|=0)} \rangle$ for $T = 0.01|\lambda|$ is so low that it is not visible. Parameters are set to $|\lambda| = 0.1\omega_c$, $\Gamma_{\text{QD}} = 4\gamma_c$, $\gamma_c = \gamma_{\text{in}} = 0.01\omega_c$, $\epsilon = -|\lambda|/2$ and with initial QD state $p^{(1)}(t = 0) = 1$ in all panels.

In summary, in the regime in which the dark count remains low, (i.e., Δn_{det} shows saturation at finite time), Eq. (17) expresses the efficiency for detecting a single photon. Moreover, high detection efficiency can be reached in the limit of low temperature and for a sufficiently fast detector monitoring the state of the QD coupled to the detection mode.

V. DISCUSSION AND EXPERIMENTAL CHALLENGES

A. Radio-frequency charge sensing

To detect single-electron charges in nanostructures, charge sensors based on quantum point contacts (QPC) or QDs have long been established as powerful tools [96, 104–106]. The operation speed and sensitivity of such sensors can be greatly enhanced by embedding them in impedance-matching resonant circuits and monitoring the reflected radio-frequency (rf) signal, a technique known as rf reflectometry [107–109]. This approach is now routinely employed for fast, high-fidelity readout of charge and spin qubits in semiconductor QDs [110]. For a broader tutorial on rf reflectometry principles, impedance matching, and backaction see Ref. [110].

An alternative QD charge detection scheme is gate-based reflectometry, where one of the confinement gates itself forms the capacitive element of the resonator and senses the QD’s quantum capacitance [111]; this eliminates the need for a separate nearby sensor. Both methods increase the charge detection bandwidth from the kHz range of dc conductance measurements up to the MHz–GHz range and enable single-shot charge or spin readout on microsecond timescales [111–114].

Using an rf single-electron transistor (rf-SET) embedded in a donor quantum-dot circuit and coupled to a resonant tank circuit operating at approximately 225 MHz, Geng *et al.* [113] demonstrated a characteristic rise–fall time constant of the charge-detector current of about 50 ns at base temperature. From signal-to-noise ratio (SNR) extrapolations, they reported an effective sensor integration time of 8 ± 1.5 ns (corresponding to $\text{SNR} = 2$) at 20 mK, establishing one of the fastest and most sensitive rf charge-detection schemes realized to date. More recently, Swift *et al.* [115] demonstrated a fully integrated, CMOS-compatible rf-SET matched via a TiN superinductor, achieving minimum integration times as short as $t_{\min} \approx 1 \pm 0.3$ ps with an estimated rise time of tens of nanoseconds—representing over two orders of magnitude improvement compared to previous rf-SET implementations.

These advances show that rf charge sensors readily achieve the bandwidth ($\gamma_{\text{det}} \sim \text{MHz–GHz}$) and SNR needed to resolve the transient QD depletion $p^{(0)}(t)$ expected from a single photon in our scheme.

B. Electron temperature and its impact on detector performance

We now briefly discuss the parameter regime experimentally accessible in hybrid circuit QED architectures with QDs, focusing on values relevant to our setup. For typical cavity frequencies of $\omega_c/(2\pi) \sim 10$ GHz, an interdot tunneling rate of $t/(2\pi) \sim 10$ GHz, and a bare charge–photon coupling of $g/(2\pi) \sim 1$ GHz—values that

are routinely achieved in state-of-the-art DQD–cavity hybrid devices [116]—the resulting dispersive coupling is $|\lambda|/(2\pi) \sim 130$ MHz (see Section A). High-quality-factor resonators with linewidths $\gamma_c/(2\pi)$ below 1 MHz have been demonstrated [117–119], placing the system well within the regime where $\gamma_c < \Gamma_{\text{QD}} < |\lambda|$, with a typical QD tunneling rate with the lead Γ_{QD} in the tens of MHz.

As discussed previously, maintaining $|\lambda|/T \gg 1$ is essential to preserve a large readout contrast. The electron temperature T of the device is a central parameter governing the efficiency of our single-photon detector. The estimated value of $|\lambda|/(2\pi)$ corresponds to a temperature of about ~ 6 mK. For semiconductor QDs, achieving and maintaining $T \lesssim 10$ mK already represents a demanding but realistic goal.

In semiconductor nanostructures, the refrigerator base temperature (10–20 mK) does not directly translate into the electronic temperature T , which typically saturates at 50–120 mK due to residual heating and the vanishing electron–phonon coupling. Substantial efforts are therefore required to reduce the electron bath temperature below this level. For instance, immersion of the device in liquid Helium, combined with extensive low-pass filtering and thermal anchoring of all electrical leads, has routinely given T of a few mK as inferred from Coulomb-blockade and QD thermometry [120–125]. Pushing further, immersion of GaAs two-dimensional electron gases in liquid 3He cooled by nuclear adiabatic demagnetisation of a copper stage has achieved sub-mK electron temperature [126, 127].

In summary, the electron temperature is a technological bottleneck for the proposed detector. The steady progress towards millikelvin and sub-millikelvin regimes demonstrates that the thermal conditions required for efficient photon-to-charge conversion are within reach of contemporary cryogenic technology, provided that the device is designed to minimize parasitic heat leaks and to exploit strong coupling between the cavity mode and the DQD.

VI. CONCLUSIONS

To summarize, we have theoretically explored a circuit QED platform for non-absorptive detection of a single propagating microwave photon, based on the dispersive coupling between a resonant cavity mode and a DQD connected to a single electronic lead. The development of a theory based on a quantum cascade approach has allowed a time-resolved description of the single-photon wavepacket incident on the cavity.

Specifically, we show how the variation of the electron level occupation is highly sensitive to the photon occupation in the regime $\gamma_c < \Gamma_{\text{QD}}$ and $T < |\lambda|$. Making use of a phenomenological model of the DQD coupled to a charge detector, we have assessed the detection efficiency of the proposed set-up. Our results demonstrate that dis-

persive interactions on hybrid circuit QED platforms can generate measurable changes in the electron level occupation that might be suitable for charge-based readout in the microwave regime.

At the same time, our analysis highlights the crucial role of temperature, which remains one of the main experimental challenges for the proposed scheme. Interestingly, the theoretical framework—valid in the Markovian limit $\Gamma_{\text{QD}} < |\lambda|$ —naturally leads to a measurement-induced backaction effect: our regime implies $|\lambda| > \gamma_c$, i.e., the dispersive coupling exceeds the cavity linewidth, thereby influencing the mechanism by which photons enter the cavity.

A promising direction for future work is to explore alternative detection schemes that offer partial immunity to thermal fluctuations. Examples include approaches based on interference effects in tunneling transport [128] or architectures relying on interdot tunneling events in buried QDs states, where the dots are well isolated from the leads by strong tunnel barriers [129]. Moreover, investigating the full counting statistics of the proposed detection protocol [130] represents an interesting and natural continuation of this work.

ACKNOWLEDGMENTS

We acknowledge continuous stimulating discussions with Christian Johansen, Anna Minguzzi, Maxime Richard, and Asian Selvakumaran. S.M., A.B., I.C. and G.R. acknowledge financial support from Provincia Autonoma di Trento (PAT); from the Q@TN Initiative; from the National Quantum Science and Technology Institute through the PNRR MUR project under Grant PE0000023-NQSTI, co-funded by the European Union – NextGeneration EU. P.S. acknowledges support from the Swiss State Secretariat for Education, Research and Innovation (SERI) under contract number MB22.00081 / REF-1131-52105 and the support from the NCCR SPIN, a National Centre of Competence in Research, funded by the Swiss National Science Foundation (SNSF) with grant number 225153. P.S. also acknowledges support from the SNSF through the grants Ref. No. 200021_200418 / 1 and Ref. No. 206021_205335 / 1.

Appendix A: Derivation of the dispersive interaction between the DQD and the resonator

1. The DQD Hamiltonian

We consider a double quantum dot (DQD) coupled to a single cavity mode via a dipole interaction described by

$$\hat{H}_{\text{QED}} = \hat{H}_{\text{DQD}} + \omega_c \hat{b}^\dagger \hat{b} + g (\hat{n}_1 - \hat{n}_2) (\hat{b} + \hat{b}^\dagger) \quad (\text{A1})$$

with

$$\hat{H}_{\text{DQD}} = \bar{\varepsilon} (\hat{n}_1 + \hat{n}_2) + \frac{\delta}{2} (\hat{n}_1 - \hat{n}_2) - t_{12} (\hat{d}_1^\dagger \hat{d}_2 + \hat{d}_2^\dagger \hat{d}_1). \quad (\text{A2})$$

Here, $\hat{n}_j = \hat{d}_j^\dagger \hat{d}_j$ are the occupations of the first ($j = 1$) and second ($j = 2$) dot, with the corresponding fermionic creation/annihilation operators $\hat{d}_j^\dagger, \hat{d}_j$. Additionally, $\bar{\varepsilon}$ is the average energy of the two dot levels, δ the DQD detuning and t_{12} is the tunnel coupling between the dots. Introducing the eigenstates of \hat{H}_{DQD} , namely the delocalized state of the electron on the two sites, we cast \hat{H}_{DQD} in terms of the fermionic operators for the ground and the excited state with one electron occupation

$$\hat{H}_{\text{DQD}} = \bar{\varepsilon} (\hat{n}_e + \hat{n}_g) + \frac{\Omega}{2} (\hat{d}_e^\dagger \hat{d}_e - \hat{d}_g^\dagger \hat{d}_g) \quad (\text{A3})$$

with the energy splitting $\Omega = \sqrt{\delta^2 + 4t_{12}^2}$ and the fermionic operators $\hat{d}_e = \cos \frac{\theta}{2} \hat{d}_1 - \sin \frac{\theta}{2} \hat{d}_2$ and $\hat{d}_g = \sin \frac{\theta}{2} \hat{d}_1 + \cos \frac{\theta}{2} \hat{d}_2$ where $\tan \theta = 2t_{12}/\delta$. We consider the case $\delta = 0$ such that the system is described by a Rabi-like model

$$\hat{H}_{\text{Rabi}} = \hat{H}_0 + \hat{H}_{\text{int}} \quad (\text{A4})$$

$$\hat{H}_0 = \bar{\varepsilon} (\hat{n}_g + \hat{n}_e) + \omega_c \hat{b}^\dagger \hat{b} + \frac{\Omega}{2} (\hat{d}_e^\dagger \hat{d}_e - \hat{d}_g^\dagger \hat{d}_g) \quad (\text{A5})$$

$$\hat{H}_{\text{int}} = g (\hat{b} + \hat{b}^\dagger) (\hat{n}_1 - \hat{n}_2) = g (\hat{b} + \hat{b}^\dagger) (\hat{\sigma}_+ + \hat{\sigma}_-). \quad (\text{A6})$$

with $\hat{\sigma}_- = \hat{d}_g^\dagger \hat{d}_e$, and $\hat{\sigma}_+ = \hat{d}_e^\dagger \hat{d}_g$. In the limit of weak interaction and far from the resonance

$$g \ll (\Omega, \omega_c), \quad g \ll |\Omega - \omega_c|, \quad (\text{A7})$$

we can apply a unitary Schrieffer-Wolff transformation to determine the effective (low-energy) Hamiltonian by decoupling weakly interacting subspaces.

With the condition $\hat{H}_{\text{int}} = - [\hat{H}_0; \hat{S}]$ one obtains to second order

$$\hat{H}' = e^{-\hat{S}} \hat{H}_{\text{Rabi}} e^{\hat{S}} \simeq \hat{H}_0 + \frac{1}{2} [\hat{H}_{\text{int}}; \hat{S}]. \quad (\text{A8})$$

Calculating the matrix elements between the unperturbed states of the Hamiltonian \hat{H}_0 , we find the operator

$$\hat{S} = \frac{g}{\Omega - \omega_c} (\hat{\sigma}_- \hat{b}^\dagger - \hat{\sigma}_+ \hat{b}) + \frac{g}{\Omega + \omega_c} (\hat{\sigma}_- \hat{b} - \hat{\sigma}_+ \hat{b}^\dagger), \quad (\text{A9})$$

and the transformed Hamiltonian corresponds to

$$\hat{H}' = \hat{H}_0 + \hat{H}_{\text{dis}} + \lambda \left(\frac{\omega_c}{\Omega} \right) \hat{\sigma}_x + \lambda (\hat{b} + \hat{b}^\dagger) \hat{\sigma}_z \quad (\text{A10})$$

with $\hat{\sigma}_x = \hat{\sigma}_+ + \hat{\sigma}_-$ and $\sigma_z = \hat{n}_e - \hat{n}_g$ and the dispersive interaction

$$\hat{H}_{\text{dis}} = \lambda [\hat{n}_e \hat{\sigma}_z + \hat{n}_g], \quad (\text{A11})$$

where [98–100]

$$\lambda = \frac{2g^2\Omega}{\Omega^2 - \omega_c^2} \left[\approx \frac{g^2}{\Omega - \omega_c} \text{ for } |\Omega - \omega_c| \ll (\Omega, \omega_c) \right]. \quad (\text{A12})$$

The $\hat{\sigma}_z$ and \hat{n} factors in dispersive coupling \hat{H}_{dis} provide a shift in opposite directions for the bonding and antibonding states of the DQD, of magnitude proportional to the photon number. Notice that we are considering the full Rabi model, so Eq. (A12) includes both the Jaynes–Cummings dispersive term as well as the Bloch–Siegert term [98–100].

The additional terms in Eq. (A10) describe further processes which are however negligible in our case. The third term proportional to the operator $\hat{\sigma}_x$ produces a mixing between the excited and the ground state that we can neglect for sufficiently large energy splitting of the electronic levels, i.e., $\Omega \gg |\lambda| (\frac{\omega_c}{\Omega})$. Moreover the fourth term in Eq. (A10) proportional to $\hat{\sigma}_z$ leads to a renormalization of the cavity mode ground state which can be included by applying an unitary polaronic transformation $\hat{U}_p = \exp\left(\frac{2g^2\Omega}{\Omega^2 - \omega_c^2}\hat{\sigma}_z\hat{b}^\dagger + \text{h.c.}\right)$. The validity of the Schrieffer–Wolff expansion holds on the condition

$$\frac{g^2}{|\Omega \pm \omega_c|} \ll (\Omega, \omega_c). \quad (\text{A13})$$

In the derivation presented here we have not assumed that the resonator frequency and the energy splitting of the DQD levels are sufficiently close to neglect the counter rotating term of the Rabi Hamiltonian [98–100]. This means that the effective dispersive Hamiltonian is also valid when, for instance, the detuning $\Delta = \Omega - \omega_c$ is comparable to frequencies of the system $\Delta \sim (\Omega, \omega_c)$.

For example, when $\omega_c = \Omega/2$, we have $\lambda = 4g^2/3\omega_c$ which corresponds to $\lambda \sim 130$ MHz for $g \sim 1$ GHz [116], as stated in the main text.

2. Reduction to a single electron level

The splitting of the two electron levels changes in presence of a photon in the cavity $\Omega \rightarrow \Omega + 2\lambda$. When coupled to a lead with chemical potential μ , one can focus on a configuration for which the variation of the splitting is important only for the occupation of one electron level, see Fig. 5 for a visualization of the energy levels used for photon detection. We set $\epsilon = \bar{\epsilon} - \Omega/2$ and $\epsilon' = \bar{\epsilon} + \Omega/2$ as the bonding and the antibonding levels.

One can impose, for example, that the antibonding state of the DQD remains empty assuming $\epsilon' > \mu$ and $\epsilon' + \lambda > \mu$, with $|\epsilon' - \mu| \gg T$ and $|\epsilon' + \lambda - \mu| \gg T$. This holds even for $|\lambda| \gg T$ since $\Omega \gg \lambda$, see Fig. 5.

Simultaneously, we can have that the bonding state occupation is strongly affected by the photon in the cavity. For $\lambda > 0$ [see Fig. 5(b)] we can assume $\epsilon > \mu$ and $\epsilon - \lambda < \mu$. For $\lambda < 0$ [see of Fig. 5(a)] we can

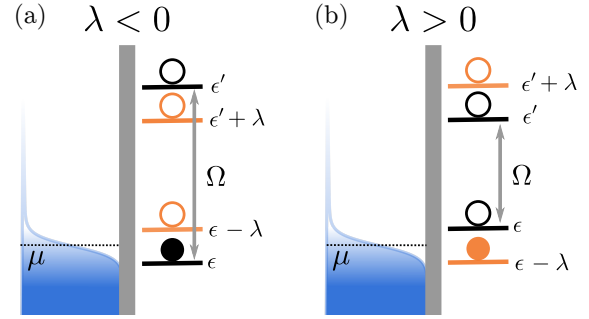


FIG. 5. Energy levels of the DQD without photon (black) and in presence of a photon (orange). The splitting between the bonding state with energy ϵ and antibonding state with energy ϵ' is given by Ω . In the presence of a photon $\Omega \rightarrow \Omega + 2\lambda$. As explained in the text of Appendix A 2 the antibonding state always remains empty for our choice of parameters whereas the bonding state is tuned such that (a) $\epsilon < \mu$ if $\lambda < 0$ (i.e., the initial state is occupied) or (b) $\epsilon > \mu$ if $\lambda > 0$ (i.e. the initial state is empty).

assume $\epsilon < \mu$ and $\epsilon - \lambda > \mu$. In the latter case ($\lambda < 0$), the bonding state of the DQD is the single effective electronic level we consider in the main text.

We summarize here the main points of the derivation presented in this Appendix: (i) we assume that the DQD detuning is zero $\delta = 0$ so that the DQD's excitation is twice the interdot tunneling amplitude t_{12} ; (ii) the coupling between the DQD and the cavity mode g approaches the ultrastrong regime $g \approx 0.1\omega_c$; (iii) the frequency detuning between the cavity mode and the DQD $|\Omega - \omega_c|$ is much larger than g ; (iv) the chemical potential of the lead is set such that in the presence of a photon, the energy level of the bonding state is shifted above ($\lambda < 0$) or below ($\lambda > 0$) the chemical potential of the lead.

Appendix B: Derivation of dissipative superoperator with the dispersive interaction

We consider the model Hamiltonian

$$\hat{H}_{\text{tot}} = \hat{H}_s + \hat{H}_{\text{tun}} + \hat{H}_{\text{lead}}. \quad (\text{B1})$$

It is composed by the system of interest, a QD dispersively coupled to a resonator (equivalent to Eq. (2) in the main text)

$$\hat{H}_s = \varepsilon_0 \hat{n}_d + \omega_0 \hat{n}_c - \lambda \hat{n}_d \hat{n}_c, \quad (\text{B2})$$

where $\hat{n}_d = \hat{d}^\dagger \hat{d}$ is the occupation of the single-level QD and \hat{d}, \hat{d}^\dagger the fermionic annihilation and creation operator, $\hat{n}_c = \hat{b}^\dagger \hat{b}$ is the occupation of the single mode resonator and \hat{b}, \hat{b}^\dagger the bosonic annihilation and creation operator, and λ the interaction strength of the dispersive coupling. We assume $\lambda < 0$ such that

$$\hat{H}_s = \varepsilon_0 \hat{n}_d + \omega_0 \hat{n}_c + |\lambda| \hat{n}_d \hat{n}_c. \quad (\text{B3})$$

The QD is tunnel-coupled to a fermionic reservoir (the contact lead), which is described by

$$\hat{H}_{\text{lead}} = \sum_k \varepsilon_k \hat{c}_k^\dagger \hat{c}_k. \quad (\text{B4})$$

The lead is modeled as a free Fermi gas with the energy dispersion ε_k and fermionic annihilation and creation op-

erators $\hat{c}_k, \hat{c}_k^\dagger$ at momentum k . Its interaction with the QD is described by the tunneling Hamiltonian

$$\hat{H}_{\text{tun}} = \left(\sum_k V_k \hat{c}_k \right) \hat{d}^\dagger + \text{h.c.} \equiv \hat{F} \hat{d}^\dagger + \text{h.c.}, \quad (\text{B5})$$

where V_k is the tunneling amplitude. In the following we use the lead operator $F = \sum_k V_k c_k$.

In the interaction picture a general operator is transformed as $\hat{O}_I(t) = e^{i\hat{H}_0 t} \hat{O} e^{-i\hat{H}_0 t}$, where $\hat{H}_0 = \hat{H}_s + \hat{H}_{\text{lead}}$. For the lead (bath) and QD (system) operators we have

$$\begin{aligned} \hat{F}_I(t) &= \sum_k V_k \hat{c}_k e^{-i\varepsilon_k t}, \\ \hat{d}_I(t) &= \hat{d} e^{-i\varepsilon_0 t} \sum_{n=0}^{+\infty} |n\rangle \langle n| e^{-in|\lambda|t} = \hat{d} e^{-i\varepsilon_0 t} \left[\hat{\Pi}_0 + \hat{\Pi}_1 e^{-i|\lambda|t} + \dots \right] \end{aligned} \quad (\text{B6})$$

where we have introduced the projector operator $\hat{\Pi}_n = |n\rangle \langle n|$ onto the Fock states of the resonator with n photons. In the following we consider the the subspace with $n = 0, 1$. The relevant projectors for $n = 0, 1$ are then given by

$$\begin{aligned} \hat{\Pi}_0 &= 1 - \hat{n}_c, \\ \hat{\Pi}_1 &= \hat{n}_c. \end{aligned} \quad (\text{B7})$$

To derive a master equation for the system's density matrix $\hat{\rho}_I = e^{i\hat{H}_s t} \hat{\rho} e^{-i\hat{H}_s t}$ in the Markovian limit we start from the Bloch-Redfield-Wangness equation

$$\frac{d\hat{\rho}_I(t)}{dt} = - \int_{-\infty}^t dt' \text{Tr}_L \left[\hat{H}_{\text{tun},I}(t) \hat{H}_{\text{tun},I}(t') \hat{\rho}_L \hat{\rho}_I(t) - \hat{H}_{\text{tun},I}(t) \hat{\rho}_L \hat{\rho}_I(t) \hat{H}_{\text{tun},I}(t') + \text{H.c.} \right], \quad (\text{B8})$$

Where Tr_L indicates the trace over the degrees of freedom of the lead. The Fermi reservoir is assumed at thermal equilibrium, such that its density matrix $\hat{\rho}_L \propto \exp(-\hat{H}_{\text{lead}}/T)$. Therefore the following correlation functions vanish

$$\langle \hat{F}(t_1) \hat{F}(t_2) \rangle_L = \langle \hat{F}^\dagger(t_1) \hat{F}^\dagger(t_2) \rangle_L = 0, \quad (\text{B9})$$

where we introduced $\langle \hat{F}(t) \hat{F}^\dagger(t') \rangle_L = \text{Tr}_L \left[\hat{F}(t) \hat{F}^\dagger(t') \hat{\rho}_L \right]$ for the correlation functions. Then, Eq. (B8) simplifies to

$$\frac{d\hat{\rho}_I(t)}{dt} = I_1 + I_2 + I_3 + I_4. \quad (\text{B10})$$

The individual terms are given by

$$I_1 = - \int_{-\infty}^t dt' R_h(t-t') \hat{d}_I^\dagger(t) \hat{d}_I(t') \hat{\rho}_I(t) + \text{H.c.}, \quad (\text{B11})$$

$$I_2 = - \int_{-\infty}^t dt' R_e^*(t-t') \hat{d}_I(t) \hat{d}_I^\dagger(t') \hat{\rho}_I(t) + \text{H.c.}, \quad (\text{B12})$$

$$I_3 = \int_{-\infty}^t dt' R_e(t-t') \hat{d}_I^\dagger(t) \hat{\rho}_I(t) \hat{d}_I(t') + \text{H.c.}, \quad (\text{B13})$$

$$I_4 = \int_{-\infty}^t dt' R_h^*(t-t') \hat{d}_I(t) \hat{\rho}_I(t) \hat{d}_I^\dagger(t') + \text{H.c.}, \quad (\text{B14})$$

where we have introduced the correlators

$$R_h(t-t') = \langle \hat{F}(t)\hat{F}^\dagger(t') \rangle_L = \sum_k |V_k|^2 [1 - f(\varepsilon_k)] e^{-i\varepsilon_k(t-t')}, \quad (\text{B15})$$

$$R_e(t-t') = \langle \hat{F}^\dagger(t')\hat{F}(t) \rangle_L = \sum_k |V_k|^2 f(\varepsilon_k) e^{-i\varepsilon_k(t-t')}, \quad (\text{B16})$$

$$R_h^*(t-t') = \langle \hat{F}(t')\hat{F}^\dagger(t) \rangle_L = \sum_k |V_k|^2 [1 - f(\varepsilon_k)] e^{i\varepsilon_k(t-t')}, \quad (\text{B17})$$

$$R_e^*(t-t') = \langle \hat{F}^\dagger(t)\hat{F}(t') \rangle_L = \sum_k |V_k|^2 f(\varepsilon_k) e^{i\varepsilon_k(t-t')}, \quad (\text{B18})$$

with the Fermi function $f(\varepsilon)$. Defining

$$\begin{aligned} R_h(E) &= \int_{-\infty}^t dt' R_h(t-t') e^{iE(t-t')} = \int_{-\infty}^t dt' \sum_k |V_k|^2 [1 - f(\varepsilon_k)] e^{i(E-\varepsilon_k)(t-t')}, \\ R_e(E) &= \int_{-\infty}^t dt' R_e(t-t') e^{iE(t-t')} \int_{-\infty}^t dt' \sum_k |V_k|^2 f(\varepsilon_k) e^{i(E-\varepsilon_k)(t-t')} \end{aligned} \quad (\text{B19})$$

and using the functional decomposition

$$\int_{-\infty}^t dt' e^{i\Omega(t-t')} = \lim_{\eta \rightarrow 0} \int_0^\infty d\tau e^{i\Omega\tau} e^{-\eta\tau} = \pi\delta(\Omega) + i\text{P}\left(\frac{1}{\Omega}\right), \quad (\text{B20})$$

one obtains

$$R_h(E) = [1 - f(E)]\Gamma(E) + i \text{Im}[R_h(E)], \quad (\text{B21})$$

$$R_e(E) = f(E)\Gamma(E) + i \text{Im}[R_e(E)], \quad (\text{B22})$$

with

$$\Gamma(E) = \pi \sum_k |V_k|^2 \delta(\varepsilon_k - E). \quad (\text{B23})$$

Hereafter we only consider the real part of the function $R_h(E)$ and $R_e(E)$ and neglect the imaginary part corresponding to a Lamb shift correction. Moreover, we assume that the tunneling rate is independent of the energy and we set $\Gamma(E) \equiv \Gamma_{\text{QD}}$. Then, the correlation functions are given by

$$R_h(E) = [1 - f(E)]\Gamma_{\text{QD}}, \quad (\text{B24})$$

$$R_e(E) = f(E)\Gamma_{\text{QD}}. \quad (\text{B25})$$

Using the time evolution of the QD operators in the single photon subspace defined in Eq. (B6) we obtain

$$\begin{aligned} I_1 &= - \int_{-\infty}^t dt' R_h(t-t') \hat{d}^\dagger \hat{d} e^{i\varepsilon_0(t-t')} [\hat{\Pi}_0 + \hat{\Pi}_1 e^{i|\lambda|(t-t')}] \hat{\rho}_I(t) + \text{H.c.} \\ &= - [R_h(\varepsilon_0) \hat{\Pi}_0 + R_h(\varepsilon_0 + |\lambda|) \hat{\Pi}_1] \hat{d}^\dagger \hat{d} \hat{\rho}_I(t) + \text{H.c.} \\ &\simeq -\Gamma_{\text{QD}} \left\{ \left[(1 - f(\varepsilon_0)) \hat{\Pi}_0 + (1 - f(\varepsilon_0 + |\lambda|)) \hat{\Pi}_1 \right] \hat{d}^\dagger \hat{d}; \hat{\rho}_I(t) \right\}. \end{aligned}$$

Similarly, we find for the remaining terms of Eq. (B10)

$$\begin{aligned} I_2 &= -\Gamma_{\text{QD}} \left\{ \left[f(\epsilon) \hat{\Pi}_0 + f(\epsilon + |\lambda|) \hat{\Pi}_1 \right] \hat{d} \hat{d}^\dagger; \hat{\rho}_I(t) \right\}, \\ I_3 &\simeq \Gamma_{\text{QD}} \left[2f(\epsilon) \hat{\Pi}_0 \hat{d}^\dagger \hat{\rho}_I(t) \hat{d} \hat{\Pi}_0 + 2f(\epsilon + |\lambda|) \hat{\Pi}_1 \hat{d}^\dagger \hat{\rho}_I(t) \hat{d} \hat{\Pi}_1 \right. \\ &\quad \left. + (f(\epsilon) + f(\epsilon + |\lambda|)) \left(\hat{\Pi}_0 \hat{d}^\dagger \hat{\rho}_I(t) \hat{d} \hat{\Pi}_1 e^{-i|\lambda|t} + \hat{\Pi}_1 \hat{d}^\dagger \hat{\rho}_I(t) \hat{d} \hat{\Pi}_0 e^{i|\lambda|t} \right) \right] \\ I_4 &\simeq \Gamma_{\text{QD}} \left[2[1 - f(\epsilon)] \hat{\Pi}_0 \hat{d} \hat{\rho}_I(t) \hat{d}^\dagger \hat{\Pi}_0 + 2[1 - f(\epsilon + |\lambda|)] \hat{\Pi}_1 \hat{d} \hat{\rho}_I(t) \hat{d}^\dagger \hat{\Pi}_1 \right. \\ &\quad \left. + (2 - f(\epsilon) - f(\epsilon + |\lambda|)) \hat{\Pi}_0 \hat{d} \hat{\rho}_I(t) \hat{d}^\dagger \hat{\Pi}_1 e^{i|\lambda|t} (2 - f(\epsilon) - f(\epsilon + |\lambda|)) \hat{\Pi}_1 \hat{d} \hat{\rho}_I(t) \hat{d}^\dagger \hat{\Pi}_0 e^{-i|\lambda|t} \right] \end{aligned} \quad (\text{B26})$$

The terms I_3 and I_4 contain an explicit time dependence. Such oscillating factors are often neglected using the secular approximation that holds if the oscillations are fast, namely $|\lambda|$ is much larger than the typical time scale evolution of the matrix elements of the density matrix, which here corresponds to Γ_{QD} . Here we do not apply the secular approximation as we consider the limit $|\lambda| \rightarrow 0$.

These oscillating factors in I_3 and I_4 of Eq. (B26) disappear when transforming the density matrix in Eq. (B10) into the Schrödinger picture, $\hat{\rho}(t) = e^{-i\hat{H}_s t} \hat{\rho}_I(t) e^{i\hat{H}_s t}$. This leads to the master equation

$$\frac{d\hat{\rho}(t)}{dt} = -i \left[\hat{H}_S; \hat{\rho}(t) \right] + \mathcal{L}_{\text{QD}} [\hat{\rho}], \quad (\text{B27})$$

where the Liouville superoperator \mathcal{L}_{QD} is given by Eq. (3) in the main text.

Appendix C: Derivation of the cascade model

The quantum cascade model was first proposed in Refs. [102, 103]. Here we give an alternative derivation. We first recover the equations of motion equivalent to Ref. [103] (interaction picture) and Ref. [102] (Heisenberg picture) and then we derive the dissipative superoperator starting from the Bloch-Redfield-Wangness equation.

We consider the following model in which two localized modes are coupled to a chiral transmission line in which the photon propagates only in one direction, with momentum $k > 0$,

$$\hat{H}_{\text{cas}} = \hat{H}_{\text{cas}}^{(0)} + \hat{H}_{\text{cas}}^{(I)}, \quad (\text{C1})$$

where

$$\hat{H}_{\text{cas}}^{(0)} = \omega_a \hat{a}^\dagger \hat{a} + \omega_b \hat{b}^\dagger \hat{b} + \int_0^\infty d\omega \omega \hat{a}_\omega^\dagger \hat{a}_\omega, \quad (\text{C2})$$

$$\hat{H}_{\text{cas}}^{(I)} = g_a (\hat{a} + \hat{a}^\dagger) \hat{\phi}(x_a) + g_b (\hat{b} + \hat{b}^\dagger) \hat{\phi}(x_b). \quad (\text{C3})$$

The field operator takes the general form

$$\hat{\phi}(x) = \int_0^\infty d\omega \phi(\omega) [\hat{a}_\omega e^{i\frac{\omega}{v}x} + \text{h.c.}], \quad (\text{C4})$$

with v the velocity of the light in the one dimensional line. Using the rotating wave approximation, we write

$$\hat{H}_{\text{cas}}^{(I)} = \int_0^\infty d\omega \phi(\omega) [g_a e^{-i\frac{\omega}{v}x_a} \hat{a} + g_b e^{-i\frac{\omega}{v}x_b} \hat{b}] \hat{a}_\omega^\dagger + \text{H.c.} \quad (\text{C5})$$

1. Equations of motion

By solving the equation of motion for the operator \hat{a}_ω in the Heisenberg picture, one finds

$$\hat{a}_\omega(t) = \hat{a}_\omega(t_0) e^{-i\omega(t-t_0)} - i \int_{t_0}^t dt' \phi(\omega) e^{-i\omega(t-t')} [g_a e^{-i\frac{\omega}{v}x_a} \hat{a}(t') + g_b e^{-i\frac{\omega}{v}x_b} \hat{b}(t')]. \quad (\text{C6})$$

Then for the operator of the bosonic mode \hat{a} the equation of motion reads

$$\frac{d\hat{a}(t)}{dt} = -i\omega_a \hat{a}(t) - g_a^2 \int_{t_0}^t dt' K(t-t') \hat{a}(t') - g_a g_b \int_{t_0}^t dt' K(t+\tau-t') \hat{b}(t') - i g_a \int_0^\infty d\omega \phi(\omega) e^{-i\omega(t-t_0)+i\frac{\omega}{v}x_a} \hat{a}_\omega, \quad (\text{C7})$$

where we set $\tau = (x_b - x_a)/v > 0$ and the response function

$$K(t-t') = \int_0^{+\infty} d\omega |\phi(\omega)|^2 e^{-i\omega(t-t')}. \quad (\text{C8})$$

For the function $K(t-t')$ we can disregard the imaginary part that lead to a weak renormalization of the eigenstates and of the spectrum. We also assume that $K(t-t')$ satisfies causality, i.e., $K = 0$ for $t' > t$. In the Markovian limit,

the function $K(t - t')$ can be treated as a δ -function provided that its characteristic time scale is faster than the typical time scale in the evolution of the operators \hat{a} and \hat{b} . In this limit, we write

$$K(t - t') \approx K_0 \delta(t - t'), \quad (\text{C9})$$

This implies that the third term appearing in Eq. (C7) vanishes since $\delta(t + \tau - t')$ the time $t + \tau$ is out of the integration range and one obtains

$$\frac{d\hat{a}(t)}{dt} = -i\omega_a \hat{a}(t) - \frac{\gamma_a}{2} \hat{a}(t) - \sqrt{\gamma_a} \hat{a}_{in}(t), \quad (\text{C10})$$

where the damping coefficients (photon losses) are defined as

$$\gamma_a = \frac{1}{2} g_a^2 K_0, \quad \gamma_b = \frac{1}{2} g_b^2 K_0, \quad (\text{C11})$$

and the noise

$$\sqrt{\gamma_a} \hat{a}_{in}(t) = -ig_a \int_0^{+\infty} d\omega \phi(\omega) e^{-i\omega(t-t_0) + i\omega x_a/v} \hat{a}_\omega, \quad (\text{C12})$$

such that $[\hat{a}_{in}(t); \hat{a}_{in}^\dagger(t')] = \delta(t - t')$. We remark that we use the Ito convention $\int_{t_0}^t dt' \delta(t - t') = 1/2$. In a similar way, one can write the equation of motion for the bosonic operator \hat{b} which reads

$$\frac{d\hat{b}(t)}{dt} = -i\omega_b \hat{b}(t) - g_b^2 \int_{t_0}^t dt' K(t - t') \hat{b}(t') - g_a g_b \int_{t_0}^t dt' K(t - \tau - t') \hat{a}(t') - ig_b \int_0^{+\infty} d\omega \phi(\omega) e^{-i\omega(t-t_0) + i\omega x_b/v} \hat{a}_\omega. \quad (\text{C13})$$

Notice that, in the third term of Eq. (C13), the time τ appears with the minus sign and therefore, in the Markovian limit, we obtain

$$\frac{d\hat{b}(t)}{dt} = -i\omega_b \hat{b}(t) - \frac{\gamma_b}{2} \hat{b}(t) - \sqrt{\gamma_b} \hat{a}_{in}(t) - \sqrt{\gamma_a \gamma_b} \hat{a}(t - \tau). \quad (\text{C14})$$

Comparing (C10) and (C14), it is evident that the resonant mode \hat{b} is affected by the field of the resonant mode \hat{a} but not viceversa.

2. Dissipative operator in the master equation

We switch to the interaction picture and we write

$$\hat{H}_{\text{cas}}^{(I)}(t) = \int_0^\infty d\omega \left[\hat{A}_\omega^\dagger(t) \hat{C}_\omega(t) + \text{H.c.} \right], \quad (\text{C15})$$

with

$$\hat{A}_\omega(t) = \phi(\omega) e^{-i\omega t} \hat{a}_\omega, \quad (\text{C16})$$

and

$$\hat{C}_\omega(t) = g_a e^{-i\frac{\omega}{v} x_a} e^{-i\omega_a t} \hat{a} + g_b e^{-i\frac{\omega}{v} x_b} e^{-i\omega_b t} \hat{b}. \quad (\text{C17})$$

Using the Born-Markov approximation, considering the coupling with the line as the interaction (perturbation), one has the equation for the density matrix of the cascade system $\hat{\rho}^{(c)}$ formed by the resonator a and b , in the interaction picture

$$\hat{\rho}_I^{(c)}(t) = e^{i\hat{H}_{\text{cas}}^{(0)} t} \hat{\rho}^{(c)}(t) e^{-i\hat{H}_{\text{cas}}^{(0)} t}. \quad (\text{C18})$$

We start from the Bloch-Redfield-Wangness equation

$$\frac{d}{dt} \hat{\rho}_I^{(c)}(t) = - \int_{-\infty}^t dt' \text{Tr}_{\text{line}} \left[\hat{H}_{\text{cas}}^{(I)}(t) \hat{H}_{\text{cas}}^{(I)}(t') \hat{\rho}_\ell \hat{\rho}_I^{(c)}(t) - \hat{H}_{\text{cas}}^{(I)}(t) \hat{\rho}_\ell \hat{\rho}_I^{(c)}(t) \hat{H}_{\text{cas}}^{(I)}(t') + \text{H.c.} \right]. \quad (\text{C19})$$

The chiral photonic 1D line is assumed to be at thermal equilibrium $\hat{\rho}_\ell^{(th)}$. In particular we consider the zero temperature limit $T = 0$ for the line, namely $\langle \hat{a}_\omega^\dagger \hat{a}_\omega \rangle = 0$ whereas $\langle \hat{a}_\omega \hat{a}_{\omega'}^\dagger \rangle = \delta(\omega - \omega')$. Then, for the non-squeezed vacuum, the following correlation function vanish

$$\begin{aligned} \text{Tr}_{\text{line}} \left[\hat{A}_\omega(t_1) \hat{A}_{\omega'}(t_2) \hat{\rho}_\ell \right] &= 0, \\ \text{Tr}_{\text{line}} \left[\hat{A}_\omega^\dagger(t_1) \hat{A}_{\omega'}^\dagger(t_2) \hat{\rho}_\ell \right] &= 0. \end{aligned} \quad (\text{C20})$$

Then, Eq. (C19) reduces to

$$\frac{d}{dt} \hat{\rho}_I^{(c)}(t) = G_1 + G_2 + G_3 + G_4, \quad (\text{C21})$$

with

$$\begin{aligned} G_1 &= - \int_{-\infty}^t dt' \int_0^\infty d\omega |\phi(\omega)|^2 e^{-i\omega\Delta t} \hat{C}_\omega^\dagger(t) \hat{C}_\omega(t') \hat{\rho}_I(t), \\ G_2 &= - \int_{-\infty}^t dt' \int_0^\infty d\omega |\phi(\omega)|^2 e^{i\omega\Delta t} \hat{\rho}_I(t) \hat{C}_\omega^\dagger(t') \hat{C}_\omega(t), \\ G_3 &= \int_{-\infty}^t dt' \int_0^\infty d\omega |\phi(\omega)|^2 e^{i\omega\Delta t} \hat{C}_\omega(t) \hat{\rho}_I(t) \hat{C}_\omega^\dagger(t'), \\ G_4 &= \int_{-\infty}^t dt' \int_0^\infty d\omega |\phi(\omega)|^2 e^{-i\omega\Delta t} \hat{C}_\omega(t') \hat{\rho}_I(t) \hat{C}_\omega^\dagger(t), \end{aligned} \quad (\text{C22})$$

where we introduced $\Delta t = t - t'$. Using the definition Eq. (C8) for the response function K , we find

$$\begin{aligned} G_1 &= - \int_{-\infty}^t dt' K(\Delta t) [g_a^2 \hat{n}_a e^{i\omega_a \Delta t} + g_b^2 \hat{n}_b e^{i\omega_b \Delta t}] \rho_I(t) - \int_{-\infty}^t dt' K(\Delta t - \tau) g_a g_b e^{i\omega_b t - i\omega_a t'} \hat{b}^\dagger \hat{a} \rho_I(t), \\ G_2 &= - \int_{-\infty}^t dt' K^*(\Delta t) \rho_I(t) [g_a^2 \hat{n}_a e^{-i\omega_a \Delta t} + g_b^2 \hat{n}_b e^{-i\omega_b \Delta t}] - \int_{-\infty}^t dt' K^*(\Delta t - \tau) g_a g_b e^{i\omega_a t' - i\omega_b t} \rho_I(t) \hat{a}^\dagger \hat{b}, \\ G_3 &= \int_{-\infty}^t dt' K^*(\Delta t) [g_a^2 e^{-i\omega_a \Delta t} \hat{a} \rho_I(t) \hat{a}^\dagger + g_b^2 e^{-i\omega_b \Delta t} \hat{b} \rho_I(t) \hat{b}^\dagger] + \int_{-\infty}^t dt' K^*(\Delta t - \tau) g_a g_b e^{-i\omega_b t + i\omega_a t'} \hat{b} \rho_I(t) \hat{a}^\dagger, \\ G_4 &= \int_{-\infty}^t dt' K(\Delta t) [g_a^2 e^{i\omega_a \Delta t} \hat{a} \rho_I(t) \hat{a}^\dagger + g_b^2 e^{i\omega_b \Delta t} \hat{b} \rho_I(t) \hat{b}^\dagger] + \int_{-\infty}^t dt' K(\Delta t - \tau) g_a g_b e^{-i\omega_a t' + i\omega_b t} \hat{a} \rho_I(t) \hat{b}^\dagger, \end{aligned}$$

where we used that the integrals containing $K(\Delta t + \tau)$ or $K^*(\Delta t + \tau)$ vanish, since $K(t - t')$ satisfies causality, i.e., $K(t - t') = 0$ for $t' > t$. Finally, we neglect the frequency and energy dependence of the Fourier transform of the function $K(t - t')$. In the Markovian limit we use Eq. (C9) and with the definitions of Eq. (C11), one obtains the master equation

$$\begin{aligned} \frac{d}{dt} \hat{\rho}_I^{(c)}(t) &= -\gamma_a \left[\left\{ \hat{a}^\dagger \hat{a}, \hat{\rho}_I^{(c)} \right\} - 2\hat{a} \hat{\rho}_I^{(c)} \hat{a}^\dagger \right] - \gamma_b \left[\left\{ \hat{b}^\dagger \hat{b}, \hat{\rho}_I^{(c)} \right\} - 2\hat{b} \hat{\rho}_I^{(c)} \hat{b}^\dagger \right] \\ &\quad - 2\sqrt{\gamma_a \gamma_b} \left[e^{-i\delta\omega t} \hat{b}^\dagger \hat{a} e^{i\omega_a \tau} \hat{\rho}_I^{(c)} + e^{i\delta\omega t} \hat{\rho}_I^{(c)} \hat{a}^\dagger \hat{b} e^{-i\omega_a \tau} \right] + 2\sqrt{\gamma_a \gamma_b} \left[e^{i\delta\omega t} \hat{b} \hat{\rho}_I^{(c)} \hat{a}^\dagger e^{-i\omega_a \tau} + e^{-i\delta\omega t} \hat{a} \hat{\rho}_I^{(c)} \hat{b}^\dagger e^{i\omega_a \tau} \right]. \end{aligned} \quad (\text{C23})$$

using the Ito convention $\int_{t_0}^t dt' \delta(t - t') = 1/2$ the frequency difference $\delta\omega = \omega_a - \omega_b$. We note that the equation for $\hat{\rho}_I^{(c)}(t)$ has an explicit time dependence appearing in the mixed terms containing both the operators of the two resonators.

Finally, we transform the density matrix from the interaction into to the Schrödinger picture

$$\hat{\rho}^{(c)}(t) = e^{-i\hat{H}_{\text{cas}}^{(0)} t} \hat{\rho}_I^{(c)}(t) e^{i\hat{H}_{\text{cas}}^{(0)} t}, \quad (\text{C24})$$

we obtain

$$\begin{aligned} \frac{d}{dt} \hat{\rho}^{(c)}(t) &= -i \left[\hat{H}_{\text{cas}}^{(0)}, \hat{\rho}^{(c)}(t) \right] - \gamma_a \left[\left\{ \hat{a}^\dagger \hat{a}, \hat{\rho}^{(c)} \right\} - 2\hat{a} \hat{\rho}^{(c)} \hat{a}^\dagger \right] - \gamma_b \left[\left\{ \hat{b}^\dagger \hat{b}, \hat{\rho}^{(c)} \right\} - 2\hat{b} \hat{\rho}^{(c)} \hat{b}^\dagger \right] \\ &\quad - 2\sqrt{\gamma_a \gamma_b} \left[\hat{b}^\dagger \hat{a} e^{i\omega_a \tau} \hat{\rho}^{(c)} + \hat{\rho}^{(c)} \hat{a}^\dagger \hat{b} e^{-i\omega_a \tau} \right] + 2\sqrt{\gamma_a \gamma_b} \left[\hat{b} \hat{\rho}^{(c)} \hat{a}^\dagger e^{-i\omega_a \tau} + \hat{a} \hat{\rho}^{(c)} \hat{b}^\dagger e^{i\omega_a \tau} \right]. \end{aligned} \quad (\text{C25})$$

In this way, the explicit time dependence appearing in Eq. (C23) for $\hat{\rho}_I^{(c)}(t)$ is removed. In a last step we apply an unitary transformation to redefine the phase of the operator \hat{a}

$$\hat{a} \longrightarrow \hat{a}_\tau = \hat{a} e^{i\omega_a \tau}. \quad (\text{C26})$$

In the following, as well as in the main text, we use \hat{a} for the bosonic operator instead of \hat{a}_τ . This corresponds to a shift of the time origin for the evolutions of the two fields which is irrelevant as long one focuses only on the dynamical properties of the mode b . The cascade master Eq. (C25) is equivalent to the one generated by the dissipator \mathcal{L}_{cas} shown in the main text in Eq. (5) changing the notation $\gamma_a \rightarrow \gamma_{\text{in}}$ and $\gamma_b \rightarrow \gamma_c$.

Appendix D: Equations for the density matrix elements and analytic formula for $\langle n_c(t) \rangle$

We define the matrix element of the density matrix as

$$\rho_{n_s n_d, \tilde{n}_s \tilde{n}_d}^{c\tilde{c}} = \langle n_s, n_d, c | \hat{\rho} | \tilde{n}_s, \tilde{n}_d, \tilde{c} \rangle, \quad (\text{D1})$$

with $n_s, \tilde{n}_s = 0, 1$ and $n_d, \tilde{n}_d = 0, 1$ the occupation number for the source and the detection mode in the single photon space, respectively, and $c, \tilde{c} = 0, 1$ are the QD's occupation states. The full system's density matrix, including both, the source and detection mode, as well as the QD, is block-diagonal. It splits into a 2×2 (zero-photon sector) and a 4×4 block (one-photon sector)

$$\hat{\rho} \rightarrow \left(\begin{array}{cc|cc|cc} \rho_{00,00}^{00} & \rho_{00,00}^{01} & 0 & 0 & 0 & 0 \\ \rho_{00,00}^{10} & \rho_{00,00}^{11} & 0 & 0 & 0 & 0 \\ \hline 0 & 0 & \rho_{01,01}^{00} & \rho_{01,01}^{01} & \rho_{01,10}^{00} & \rho_{01,10}^{01} \\ 0 & 0 & \rho_{01,01}^{10} & \rho_{01,01}^{11} & \rho_{01,10}^{10} & \rho_{01,10}^{11} \\ \hline 0 & 0 & \rho_{10,01}^{00} & \rho_{10,01}^{01} & \rho_{10,10}^{00} & \rho_{10,10}^{01} \\ 0 & 0 & \rho_{10,01}^{10} & \rho_{10,01}^{11} & \rho_{10,10}^{10} & \rho_{10,10}^{11} \end{array} \right). \quad (\text{D2})$$

The full equations of motion for each component of the density matrix are generated by Eq. (6).

First, we first consider the components diagonal with respect to a photon in the source mode $\rho_{10,10}^{00}$ and $\rho_{10,10}^{11}$. We only report the diagonal elements with respect to charge as the off-diagonal entries, $\rho_{10,10}^{cc'}$ with $(c \neq c')$, are decoupled from the diagonal ones, as for a single QD. This also holds for the other sub-blocks with different photon occupation. The corresponding equations read

$$\begin{aligned} \dot{\rho}_{10,10}^{00} &= -(f(\epsilon)\Gamma_{\text{QD}} + 2\gamma_{\text{in}})\rho_{10,10}^{00} + (1-f(\epsilon))\Gamma_{\text{QD}}\rho_{10,10}^{11}, \\ \dot{\rho}_{10,10}^{11} &= f(\epsilon)\Gamma_{\text{QD}}\rho_{10,10}^{00} - [(1-f(\epsilon))\Gamma_{\text{QD}} + 2\gamma_{\text{in}}]\rho_{10,10}^{11}. \end{aligned} \quad (\text{D3})$$

The coupled equations for $\rho_{10,10}^{00}$ and $\rho_{10,10}^{11}$ are closed as expected from the unidirectional interaction between source and detection mode. Using the initial conditions, $\rho_{10,10}^{00}(t=0) = 0, \rho_{10,10}^{11}(t=0) = 1$ and $p^{(1)}(t=0) = 1$, the factorized solutions are

$$\begin{aligned} \rho_{10,10}^{00}(t) &= e^{-2\gamma_{\text{in}}t} (1 - e^{-\Gamma_{\text{QD}}t}) (1 - f(\epsilon)), \\ \rho_{10,10}^{11}(t) &= e^{-2\gamma_{\text{in}}t} [e^{-\Gamma_{\text{QD}}t} (1 - f(\epsilon)) + f(\epsilon)]. \end{aligned} \quad (\text{D4})$$

From this we find the average occupation of the source mode

$$\langle \hat{n}_{\text{in}}(t) \rangle = \rho_{10,10}^{00}(t) + \rho_{10,10}^{11}(t) = e^{-2\gamma_{\text{in}}t}, \quad (\text{D5})$$

as show in Fig. 2. This solution is independent of the initial choice $\rho_{10,10}^{00}(t=0), \rho_{10,10}^{11}(t=0)$, as long as $\rho_{10,10}^{00}(t=0) + \rho_{10,10}^{11}(t=0) = 1$ holds.

Second, we consider the equations for the blocks with off-diagonal photon states (photon coherence), $\rho_{10,01}^{00}$ and $\rho_{10,01}^{11}$.

For those, we find

$$\begin{aligned}\dot{\rho}_{10,01}^{00} &= -2\sqrt{\gamma_{\text{in}}\gamma_c}\rho_{10,10}^{00} - \left[\frac{\Gamma_{\text{QD}}}{2} (f(\epsilon) + f(\epsilon + |\lambda|)) + (\gamma_{\text{in}} + \gamma_c + i\Delta\omega) \right] \rho_{10,01}^{00} + \frac{\Gamma_{\text{QD}}}{2} (2 - f(\epsilon) - f(\epsilon + |\lambda|)) \rho_{10,01}^{11}, \\ \dot{\rho}_{10,01}^{11} &= -2\sqrt{\gamma_{\text{in}}\gamma_c}\rho_{10,10}^{11} + \frac{\Gamma_{\text{QD}}}{2} (f(\epsilon) + f(\epsilon + |\lambda|)) \rho_{10,01}^{00} - \left[\frac{\Gamma_{\text{QD}}}{2} (2 - f(\epsilon) - f(\epsilon + |\lambda|)) + (\gamma_{\text{in}} + \gamma_c + i(\Delta\omega - |\lambda|)) \right] \rho_{10,01}^{11}.\end{aligned}\quad (\text{D6})$$

The equations for $\rho_{01,10}^{00}$ and $\rho_{01,10}^{11}$ are given by the complex conjugate of Eq. (D6).

Third, we consider the components diagonal with respect to a having a photon in the detection mode,

$$\begin{aligned}\dot{\rho}_{01,01}^{00} &= -4\sqrt{\gamma_{\text{in}}\gamma_c} \text{Re} \{ \rho_{10,01}^{00} \} - (\Gamma_{\text{QD}} f(\epsilon + |\lambda|) + 2\gamma_c) \rho_{01,01}^{00} + \Gamma_{\text{QD}} (1 - f(\epsilon + |\lambda|)) \rho_{01,01}^{11}, \\ \dot{\rho}_{01,01}^{11} &= -4\sqrt{\gamma_{\text{in}}\gamma_c} \text{Re} \{ \rho_{10,01}^{11} \} + \Gamma_{\text{QD}} f(\epsilon + |\lambda|) \rho_{01,01}^{00} - [\Gamma_{\text{QD}} (1 - f(\epsilon + |\lambda|)) + 2\gamma_c] \rho_{01,01}^{11}.\end{aligned}\quad (\text{D7})$$

From this, one finds the equation of motion for the occupation of the detection mode

$$\frac{d}{dt} \langle n_c(t) \rangle = \dot{\rho}_{01,01}^{00} + \dot{\rho}_{01,01}^{11}. \quad (\text{D8})$$

This shows the dependence of $\langle n_c(t) \rangle$ on the coherence between source and detection mode (first term in the equation of motion of $\rho_{01,01}^{00}$ and $\rho_{01,01}^{11}$ in Eq. (D7)).

Solving the equations of motion of Eq. (D6), and inserting the solutions into Eq. (D8) leads to an involved expression for $\langle \hat{n}_c(t) \rangle$. We state here the closed form solution for $T \rightarrow 0, \Delta\omega = |\lambda|, \gamma_{\text{in}} = \gamma_c$, which is given by

$$\begin{aligned}\langle \hat{n}_c(t) \rangle &= \frac{16\gamma_c^2}{\Gamma_{\text{QD}}^2} e^{-2t\gamma_c} (t\Gamma_{\text{QD}} - 2) + \frac{16\gamma_c^2}{|\lambda|^2} e^{-2t\gamma_c} \\ &\quad - \frac{16\gamma_c^2}{\Gamma_{\text{QD}}^2 |\lambda|^2} e^{-2t\gamma_c - t\Gamma_{\text{QD}}/2} \cosh \left(\frac{t}{2} \sqrt{\Gamma_{\text{QD}}^2 - |\lambda|^2} \right) [2(\Gamma_{\text{QD}}^2 - |\lambda|^2) \cos(t|\lambda|/2) + 3|\lambda|\Gamma_{\text{QD}} \sin(t|\lambda|/2)] \\ &\quad + \frac{16\gamma_c^2}{\Gamma_{\text{QD}}^2 |\lambda|^2} e^{-2t\gamma_c - t\Gamma_{\text{QD}}/2} \frac{\sinh \left(\frac{t}{2} \sqrt{\Gamma_{\text{QD}}^2 - |\lambda|^2} \right)}{\sqrt{\Gamma_{\text{QD}}^2 - |\lambda|^2}} [\Gamma_{\text{QD}} (3|\lambda|^2 - 2\Gamma_{\text{QD}}^2) \cos(t|\lambda|/2) + |\lambda| (2|\lambda|^2 - 3\Gamma_{\text{QD}}^2) \sin(t|\lambda|/2)].\end{aligned}\quad (\text{D9})$$

In the limit $|\lambda| \rightarrow 0$ (independent of T), i.e, the QD system is decoupled from the photon, the general solution of Eq. (D8) yields

$$\begin{aligned}\langle \hat{n}_c(t) \rangle^{(|\lambda|=0)} &= \frac{8\gamma_{\text{in}}\gamma_c e^{-2t(\gamma_{\text{in}}+\gamma_c)}}{(\gamma_{\text{in}} - \gamma_c)^2 + \Delta\omega^2} \{ \cosh[(\gamma_{\text{in}} - \gamma_c)t] - \cos(\Delta\omega t) \} \\ &= \begin{cases} 4t^2\gamma_c^2 e^{-2t\gamma_c} & \text{for } \gamma_{\text{in}} = \gamma_c, \Delta\omega = 0 \\ \frac{16\gamma_c^2}{\Delta\omega^2} \sin^2(t\Delta\omega/2) e^{-2\gamma_c t} & \text{for } \gamma_{\text{in}} = \gamma_c, \Delta\omega \neq 0 \end{cases}.\end{aligned}\quad (\text{D10})$$

For the optimal conditions of maximum photon occupation of the detection mode, i.e., $\gamma_{\text{in}} = \gamma_c$ and $\Delta\omega = 0$, the maximum is $\langle n_c \rangle_{\text{opt,max}}^{(|\lambda|=0)} = 4/e^2$ is at $t = 1/\gamma_c$. The impact of the detuning becomes apparent from the prefactor $(16\gamma_c^2/\Delta\omega^2)$ that suppress the detection mode occupation. A similar prefactor $(16\gamma_c^2/|\lambda|^2)$ appears in Eq. (D9) for $\langle \hat{n}_c \rangle(t)$ when $\Delta\omega = |\lambda|$, supporting the idea that the dispersive interaction suppresses the occupation by dynamically detuning the detection mode from resonance. Note that Eq. (D9) to zeroth order in $|\lambda|$ and Γ_{QD} reduces to Eq. (D10) for $(\gamma_{\text{in}} = \gamma_c$ and $\Delta\omega = 0$, i.e, $\langle \hat{n}_c(t) \rangle = \langle n_c(t) \rangle_{\text{opt}}^{(|\lambda|=0)} + \mathcal{O}(|\lambda|, \Gamma_{\text{QD}})$.

In the limit of $|\lambda| \rightarrow \infty$ (and $T \rightarrow 0, \gamma_{\text{in}} = \gamma_c$) we find for $\Delta\omega = |\lambda|$ that

$$\langle n_c(t) \rangle^{(|\lambda| \rightarrow \infty)} = \frac{16\gamma_c^2}{\Gamma_{\text{QD}}^2} e^{-\frac{t}{2}(4\gamma_c + \Gamma_{\text{QD}})} \left[2 + e^{\frac{t}{2}\Gamma_{\text{QD}}} (t\Gamma_{\text{QD}} - 2) \right], \quad (\text{D11})$$

and its maximum

$$\langle n_c \rangle_{\text{max}}^{(|\lambda| \rightarrow \infty)} = \frac{8\gamma_c}{\Gamma_{\text{QD}} (4\gamma_c + \Gamma_{\text{QD}})} e^{-(4\gamma_c + \Gamma_{\text{QD}} + 4\gamma_c W(z))/\Gamma_{\text{QD}}} [4\gamma_c + \Gamma_{\text{QD}} + 4\gamma_c W(z)], \quad (\text{D12})$$

where $W(z)$ is the Lambert W function at $z = -\exp[-1 - \Gamma_{\text{QD}}/4\gamma_c] (4\gamma_c + \Gamma_{\text{QD}})/4\gamma_c$.

For completeness, we report the equation for the zero-photon subspace, diagonal in the QD charge

$$\begin{aligned}\dot{\rho}_{00,00}^{00} &= \Gamma_{\text{QD}} [\rho_{00,00}^{11} - f(\epsilon) (\rho_{00,00}^{00} + \rho_{00,00}^{11})] + 2 [\gamma_{\text{in}} \rho_{10,10}^{00} + 2\sqrt{\gamma_{\text{in}} \gamma_c} \text{Re} \{ \rho_{10,01}^{00} \} + \gamma_c \rho_{01,01}^{00}], \\ \dot{\rho}_{00,00}^{11} &= \Gamma_{\text{QD}} [f(\epsilon) (\rho_{00,00}^{00} + \rho_{00,00}^{11}) - \rho_{00,00}^{11}] + 2 [\gamma_{\text{in}} \rho_{10,10}^{11} + 2\sqrt{\gamma_{\text{in}} \gamma_c} \text{Re} \{ \rho_{10,01}^{11} \} + \gamma_c \rho_{01,01}^{11}].\end{aligned}\quad (\text{D13})$$

From the solutions for all the components with photons, one can in turn find the solutions for the zero-photon sector in Eq. (D13), and finally for the occupation of the QD

$$\begin{aligned}p^{(0)} &= \rho_{00,00}^{00} + \rho_{10,10}^{00} + \rho_{01,01}^{00}, \\ p^{(1)} &= \rho_{00,00}^{11} + \rho_{10,10}^{11} + \rho_{01,01}^{11}.\end{aligned}\quad (\text{D14})$$

[1] S. Haroche, M. Brune, and J. M. Raimond, From cavity to circuit quantum electrodynamics, *Nat. Phys.* **16**, 243 (2020).

[2] A. Blais, A. L. Grimsom, S. M. Girvin, and A. Wallraff, Circuit quantum electrodynamics, *Rev. Mod. Phys.* **93**, 025005 (2021).

[3] X. Gu, A. Kockum, A. L.-x. Miranowicz, and F. Nori, Microwave photonics with superconducting quantum circuits, *Phys. Rep.* **718**, 1 (2017).

[4] R. H. Hadfield, Single-photon detectors for optical quantum information applications, *Nat. Photonics* **3**, 696 (2009).

[5] L. Mandel and E. Wolf, *Optical coherence and quantum optics* (Cambridge university press, 1995).

[6] D. Walls and G. J. Milburn, Quantum optics and quantum foundations, in *Quantum Optics* (Springer, 2025) pp. 225–244.

[7] P. Kok, W. J. Munro, K. Nemoto, T. C. Ralph, J. P. Dowling, and G. J. Milburn, Linear optical quantum computing with photonic qubits, *Rev. Mod. Phys.* **79**, 135 (2007).

[8] S. L. Hermans, M. Pompili, L. D. S. Martins, A. R. Montblanch, H. K. Beukers, S. Baier, J. Borregaard, and R. Hanson, Entangling remote qubits using the single-photon protocol: an in-depth theoretical and experimental study, *New J. Phys.* **25**, 013011 (2023).

[9] Y.-F. Chen, D. Hover, S. Sendelbach, L. Maurer, S. T. Merkel, E. J. Pritchett, F. K. Wilhelm, and R. McDermott, Microwave photon counter based on Josephson junctions, *Phys. Rev. Lett.* **107**, 217401 (2011).

[10] G. Oelsner, L. S. Revin, E. Il'ichev, A. L. Pankratov, H.-G. Meyer, L. Grönberg, J. Hassel, and L. S. Kuzmin, Underdamped Josephson junction as a switching current detector, *Appl. Phys. Lett.* **103**, 142605 (2013).

[11] G. Oelsner, C. K. Andersen, M. Rehák, M. Schmelz, S. Anders, M. Grajcar, U. Hübner, K. Mølmer, and E. Il'ichev, Detection of weak microwave fields with an underdamped Josephson junction, *Phys. Rev. Appl.* **7**, 014012 (2017).

[12] L. S. Kuzmin, A. S. Sobolev, C. Gatti, D. Di Gioacchino, N. Crescini, A. Gordeeva, and E. Il'ichev, Single photon counter based on a Josephson junction at 14 GHz for searching galactic axions, *IEEE Trans. Appl. Supercond.* **28**, 2400505 (2018).

[13] L. S. Revin, A. L. Pankratov, A. V. Gordeeva, A. A. Yablokov, I. V. Rakut, V. O. Zbrozhek, and L. S. Kuzmin, Microwave photon detection by an Al Josephson junction, *Beilstein J. Nanotechnol.* **11**, 960 (2020).

[14] A. L. Pankratov, L. S. Revin, A. V. Gordeeva, A. A. Yablokov, L. S. Kuzmin, and E. Il'ichev, Towards a microwave single-photon counter for searching axions, *npj Quantum Inf.* **8**, 61 (2022).

[15] A. D'Elia, A. Rettaroli, S. Tocci, D. Babusci, C. Barone, M. Beretta, B. Buonomo, F. Chiarello, N. Chikhi, D. Di Gioacchino, G. Felici, G. Filatrella, M. Fistul, L. Foggetta, C. Gatti, E. Il'ichev, C. Ligi, M. Lisitskiy, G. Maccarrone, F. Mattioli, G. Oelsner, S. Pagano, L. Piersanti, B. Ruggiero, G. Torrioli, and A. Zagorskin, Stepping closer to pulsed single microwave photon detectors for axions search, *IEEE Trans. Appl. Supercond.* **33**, 1 (2023).

[16] A. Poudel, R. McDermott, and M. G. Vavilov, Quantum efficiency of a microwave photon detector based on a current-biased Josephson junction, *Phys. Rev. B* **86**, 174506 (2012).

[17] C. K. Andersen and K. Mølmer, Effective description of tunneling in a time-dependent potential with applications to voltage switching in Josephson junctions, *Phys. Rev. A* **87**, 052119 (2013).

[18] C. K. Andersen, G. Oelsner, E. Il'ichev, and K. Mølmer, Quantized resonator field coupled to a current-biased Josephson junction in circuit QED, *Phys. Rev. A* **89**, 033853 (2014).

[19] D. S. Golubev, E. V. Il'ichev, and L. S. Kuzmin, Single-photon detection with a Josephson junction coupled to a resonator, *Phys. Rev. Appl.* **16**, 014025 (2021).

[20] A. Opremcak, I. V. Pechenezhskiy, C. Howington, B. G. Christensen, M. A. Beck, E. Leonard Jr., J. Suttle, C. Wilen, K. N. Nesterov, G. J. Ribeill, T. Thorbeck, F. Schlenker, M. G. Vavilov, B. L. T. Plourde, and R. McDermott, Measurement of a superconducting qubit with a microwave photon counter, *Science* **361**, 1239 (2018).

[21] A. Opremcak, C. H. Liu, C. Wilen, K. Okubo, B. G. Christensen, D. Sank, T. C. White, A. Vainsencher, M. Giustina, A. Megrant, B. Burkett, B. L. T. Plourde, and R. McDermott, High-fidelity measurement of a superconducting qubit using an on-chip microwave photon counter, *Phys. Rev. X* **11**, 011027 (2021).

[22] K. Petrovnik, J. Wang, M. Perelshtain, P. Hakonen, and G. S. Paraoanu, Microwave photon detection at parametric criticality, *PRX Quantum* **5**, 020342 (2024).

[23] K. Koshino, Down-conversion of a single photon with unit efficiency, *Phys. Rev. A* **79**, 013804 (2009).

[24] K. Koshino, K. Inomata, T. Yamamoto, and Y. Nakamura, Implementation of an impedance-matched Λ system by dressed-state engineering, *Phys. Rev. Lett.* **111**, 153601 (2013).

[25] K. Koshino, K. Inomata, Z. Lin, Y. Nakamura, and T. Yamamoto, Theory of microwave single-photon detection using an impedance-matched Λ system, *Phys. Rev. A* **91**, 043805 (2015).

[26] K. Inomata, Z. Lin, K. Koshino, W. D. Oliver, J.-S. Tsai, T. Yamamoto, and Y. Nakamura, Single microwave-photon detector using an artificial Λ -type three-level system, *Nat. Commun.* **7**, 12303 (2016).

[27] O. Stanisavljević, J.-C. Philippe, J. Gabelli, M. Aprili, J. Estève, and J. Basset, Efficient microwave photon-to-electron conversion in a high-impedance quantum circuit, *Phys. Rev. Lett.* **133**, 076302 (2024).

[28] J. Basset, O. Stanisavljević, J. Gabelli, M. Aprili, and J. Estève, Fast and continuous detection of single microwave photons via photo-assisted quasiparticle tunneling to a superconducting island (2025), arXiv:2511.17470.

[29] R. Lescanne, S. Deléglise, E. Albertinale, U. Réglade, T. Capelle, E. Ivanov, T. Jacqmin, Z. Leghtas, and E. Flurin, Irreversible qubit-photon coupling for the detection of itinerant microwave photons, *Phys. Rev. X* **10**, 021038 (2020).

[30] E. Albertinale, L. Balembois, E. Billaud, V. Ranjan, D. Flanigan, T. Schenkel, D. Estève, D. Vion, P. Bertet, and E. Flurin, Detecting spins by their fluorescence with a microwave photon counter, *Nature* **600**, 434 (2021).

[31] Z. Wang, L. Balembois, M. E. Rančić, M. and Billaud, M. Le Dantec, A. Ferrier, P. Goldner, S. Bertaina, T. Chanelière, D. Esteve, D. Vion, P. Bertet, and E. Flurin, Single-electron spin resonance detection by microwave photon counting, *Nature* **619**, 276 (2023).

[32] E. Billaud, L. Balembois, M. Le Dantec, M. Rančić, E. Albertinale, S. Bertaina, T. Chanelière, P. Goldner, D. Estève, D. Vion, P. Bertet, and E. Flurin, Microwave fluorescence detection of spin echoes, *Phys. Rev. Lett.* **131**, 100804 (2023).

[33] C. Braggio, L. Balembois, R. Di Vora, Z. Wang, J. Travessedo, L. Pallegoix, G. Carugno, A. Ortolan, G. Russo, U. Gambardella, D. D'Agostino, P. Bertet, and E. Flurin, Quantum-enhanced sensing of axion dark matter with a transmon-based single microwave photon counter, *Phys. Rev. X* **15**, 021031 (2025).

[34] J. Govenius, R. E. Lake, K. Y. Tan, and M. Möttönen, Detection of zeptojoule microwave pulses using electrothermal feedback in proximity-induced josephson junctions, *Phys. Rev. Lett.* **117**, 030802 (2016).

[35] R. Kokkonemi, J.-P. Girard, D. Hazra, A. Laitinen, J. Govenius, R. E. Lake, I. Sallinen, V. Vesterinen, M. Partanen, J. Y. Tan, K. W. Chan, K. Y. Tan, P. Hakonen, and M. Möttönen, Bolometer operating at the threshold for circuit quantum electrodynamics, *Nature* **586**, 47 (2020).

[36] G.-H. Lee, D. K. Efetov, W. Jung, L. Ranzani, E. D. Walsh, T. A. Ohki, T. Taniguchi, K. Watanabe, P. Kim, D. Englund, and K. C. Fong, Graphene-based Josephson junction microwave bolometer, *Nature* **586**, 42 (2020).

[37] S. Kono, K. Koshino, Y. Tabuchi, A. Noguchi, and Y. Nakamura, Quantum non-demolition detection of an itinerant microwave photon, *Nature Phys.* **14**, 546 (2018).

[38] J.-C. Besse, S. Gasparinetti, M. C. Collodo, T. Waller, P. Kurpiers, M. Pechal, C. Eichler, and A. Wallraff, Single-shot quantum nondemolition detection of individual itinerant microwave photons, *Phys. Rev. X* **8**, 021003 (2018).

[39] A. Narla, S. Shankar, M. Hatridge, Z. Leghtas, K. M. Sliwa, E. Zalys-Geller, S. O. Mundhada, W. Pfaff, L. Frunzio, R. J. Schoelkopf, and M. H. Devoret, Robust concurrent remote entanglement between two superconducting qubits, *Phys. Rev. X* **6**, 031036 (2016).

[40] A. Chatterjee, P. Stevenson, S. De Franceschi, A. Morello, N. P. de Leon, and F. Kuemmeth, Semiconductor qubits in practice, *Nat. Rev. Phys.* **3**, 157 (2021).

[41] X. Zhang, H.-O. Li, G. Cao, M. Xiao, G.-C. Guo, and G.-P. Guo, Semiconductor quantum computation, *Natl. Sci. Rev.* **6**, 32 (2019).

[42] G. Burkard, T. D. Ladd, A. Pan, J. M. Nichol, and J. R. Petta, Semiconductor spin qubits, *Rev. Mod. Phys.* **95**, 025003 (2023).

[43] A. Cottet, M. Dartiaih, M. Desjardins, T. Cubaynes, L. Contamin, M. Delbecq, J. Viennot, L. Bruhat, B. Douçot, and T. Kontos, Cavity QED with hybrid nanocircuits: from atomic-like physics to condensed matter phenomena, *J. Phys. Condens. Matter* **29**, 433002 (2017).

[44] G. Burkard, M. J. Gullans, X. Mi, and J. R. Petta, Superconductor-semiconductor hybrid-circuit quantum electrodynamics, *Nat. Rev. Phys.* **2**, 129 (2020).

[45] T. Frey, P. J. Leek, M. Beck, A. Blais, T. Ihn, K. Ensslin, and A. Wallraff, Dipole coupling of a double quantum dot to a microwave resonator, *Phys. Rev. Lett.* **108**, 046807 (2011).

[46] M. R. Delbecq, V. Schmitt, F. D. Parmentier, N. Roch, J. J. Viennot, G. Fève, B. Huard, C. Mora, A. Cottet, and T. Kontos, Coupling a quantum dot, fermionic leads, and a microwave cavity on a chip, *Phys. Rev. Lett.* **107**, 256804 (2011).

[47] K. D. Petersson, L. W. McFaul, M. D. Schroer, M. Jung, J. M. Taylor, A. A. Houck, and J. R. Petta, Circuit quantum electrodynamics with a spin qubit, *Nature* **490**, 380 (2012).

[48] J. Basset, D.-D. Jarausch, A. Stockklauser, T. Frey, C. Reichl, W. Wegscheider, T. M. Ihn, K. Ensslin, and A. Wallraff, Single-electron double quantum dot dipole-coupled to a single photonic mode, *Phys. Rev. B* **88**, 125312 (2013).

[49] F. R. Braakman, J. Danon, L. R. Schreiber, W. Wegscheider, and L. M. K. Vandersypen, Dynamics of spin-flip photon-assisted tunneling, *Phys. Rev. B* **89**, 075417 (2014).

[50] C. Rössler, D. Oehri, O. Zilberberg, G. Blatter, M. Karalic, J. Pijnenburg, A. Hofmann, T. Ihn, K. Ensslin, C. Reichl, and W. Wegscheider, Transport spectroscopy of a spin-coherent dot-cavity system, *Phys. Rev. Lett.* **115**, 166603 (2015).

[51] J. J. Viennot, M. C. Dartiaih, A. Cottet, and T. Kontos, Coherent coupling of a single spin to microwave cavity photons, *Science* **349**, 408 (2015).

[52] V. Ranjan, G. Puebla-Hellmann, M. Jung, T. Hasler, A. Nunnenkamp, M. Muoth, C. Hierold, A. Wallraff, and C. Schönenberger, Clean carbon nanotubes coupled

to superconducting impedance-matching circuits, *Nat. Commun.* **6**, 7165 (2015).

[53] J. Viennot, M. R. Delbecq, L. E. Bruhat, M. C. Dartailh, M. M. Desjardins, M. Baillergeau, A. Cottet, and T. Kontos, Towards hybrid circuit quantum electrodynamics with quantum dots, *Comptes Rendus Physique* **17**, 705 (2016).

[54] F. Beaudoin, D. Lachance-Quirion, W. Coish, and M. Pioro-Ladrière, Coupling a single electron spin to a microwave resonator: controlling transverse and longitudinal couplings, *Nanotechnology* **27**, 464003 (2016).

[55] L. E. Bruhat, J. J. Viennot, M. C. Dartailh, M. M. Desjardins, T. Kontos, and A. Cottet, Cavity photons as a probe for charge relaxation resistance and photon emission in a quantum dot coupled to normal and superconducting continua, *Phys. Rev. X* **6**, 021014 (2016).

[56] T. Brandes and N. Lambert, Steering of a bosonic mode with a double quantum dot, *Phys. Rev. B* **67**, 125323 (2003).

[57] L. Childress, A. S. Sørensen, and M. D. Lukin, Mesoscopic cavity quantum electrodynamics with quantum dots, *Phys. Rev. A* **69**, 042302 (2004).

[58] M. Trif, V. N. Golovach, and D. Loss, Spin dynamics in InAs nanowire quantum dots coupled to a transmission line, *Phys. Rev. B* **77**, 045434 (2008).

[59] A. Cottet and T. Kontos, Spin quantum bit with ferromagnetic contacts for circuit QED, *Phys. Rev. Lett.* **105**, 160502 (2010).

[60] A. Cottet, T. Kontos, and A. L. Yeyati, Subradiant split Cooper pairs, *Phys. Rev. Lett.* **108**, 166803 (2012).

[61] P.-Q. Jin, M. Marthaler, A. Shnirman, and G. Schön, Strong coupling of spin qubits to a transmission line resonator, *Phys. Rev. Lett.* **108**, 190506 (2012).

[62] X. Hu, Y.-x. Liu, and F. Nori, Strong coupling of a spin qubit to a superconducting stripline cavity, *Phys. Rev. B* **86**, 035314 (2012).

[63] C. Bergenfeldt and P. Samuelsson, Nonlocal transport properties of nanoscale conductor-microwave cavity systems, *Phys. Rev. B* **87**, 195427 (2013).

[64] L. D. Contreras-Pulido, C. Emery, T. Brandes, and R. Aguado, Non-equilibrium correlations and entanglement in a semiconductor hybrid circuit QED system, *New J. Phys.* **15**, 095008 (2013).

[65] C. Kloeffel, M. Trif, P. Stano, and D. Loss, Circuit QED with hole-spin qubits in Ge/Si nanowire quantum dots, *Phys. Rev. B* **88**, 241405 (2013).

[66] C. Bergenfeldt, P. Samuelsson, B. Sothmann, C. Flindt, and M. Büttiker, Hybrid microwave-cavity heat engine, *Phys. Rev. Lett.* **112**, 076803 (2014).

[67] A. Cottet, T. Kontos, and B. Douçot, Electron-photon coupling in mesoscopic quantum electrodynamics, *Phys. Rev. B* **91**, 205417 (2015).

[68] O. Dmytruk, M. Trif, C. Mora, and P. Simon, Out-of-equilibrium quantum dot coupled to a microwave cavity, *Phys. Rev. B* **93**, 075425 (2016).

[69] A. Cottet, Z. Leghtas, and T. Kontos, Theory of interactions between cavity photons induced by a mesoscopic circuit, *Phys. Rev. B* **102**, 155105 (2020).

[70] M. Governale, C. Schönenberger, P. Scarlino, and G. Rastelli, Entangled photon-pair emission in waveguide circuit QED from a Cooper pair splitter, *PRX Quantum* **6**, 020339 (2025).

[71] F. Hellbach, F. Pauly, W. Belzig, and G. Rastelli, Quantum-correlated photons generated by nonlocal electron transport, *Phys. Rev. B* **105**, L241407 (2022).

[72] G. Rastelli and M. Governale, Single atom laser in normal-superconductor quantum dots, *Phys. Rev. B* **100**, 085435 (2019).

[73] M. Mantovani, A. D. Armour, W. Belzig, and G. Rastelli, Dynamical multistability in a quantum-dot laser, *Phys. Rev. B* **99**, 045442 (2019).

[74] M. Mantovani, W. Belzig, G. Rastelli, and R. Hussein, Single-photon pump by Cooper-pair splitting, *Phys. Rev. Res.* **1**, 033098 (2019).

[75] X. Mi, J. V. Cady, D. M. Zajac, P. W. Deelman, and J. R. Petta, Strong coupling of a single electron in silicon to a microwave photon, *Science* **355**, 156 (2016).

[76] A. Stockklauser, P. Scarlino, J. V. Koski, S. Gasparinetti, C. K. Andersen, C. Reichl, W. Wegscheider, T. Ihn, K. Ensslin, and A. Wallraff, Strong Coupling Cavity QED with Gate-Defined Double Quantum Dots Enabled by a High Impedance Resonator, *Phys. Rev. X* **7**, 011030 (2017).

[77] X. Mi, J. V. Cady, D. M. Zajac, J. Stehlík, L. F. Edge, and J. R. Petta, Circuit quantum electrodynamics architecture for gate-defined quantum dots in silicon, *Appl. Phys. Lett.* **110**, 043502 (2017).

[78] P. Scarlino, D. J. van Woerkom, A. Stockklauser, J. V. Koski, M. C. Collodo, S. Gasparinetti, C. Reichl, W. Wegscheider, T. Ihn, K. Ensslin, and A. Wallraff, All-microwave control and dispersive readout of gate-defined quantum dot qubits in circuit quantum electrodynamics, *Phys. Rev. Lett.* **122**, 206802 (2019).

[79] Y. Li, S.-X. Li, F. Gao, H.-O. Li, G. Xu, K. Wang, D. Liu, G. Cao, M. Xiao, T. Wang, J.-J. Zhang, G.-C. Guo, and G.-P. Guo, Coupling a germanium hut wire hole quantum dot to a superconducting microwave resonator, *Nano Letters* **18**, 2091 (2018).

[80] N. Samkharadze, G. Zheng, N. Kalhor, D. Brousse, A. Sammak, U. C. Mendes, A. Blais, G. Scappucci, and L. M. K. Vandersypen, Strong spin-photon coupling in silicon, *Science* **359**, 1123 (2018).

[81] X. Mi, M. Benito, S. Putz, D. M. Zajac, J. M. Taylor, G. Burkard, and J. R. Petta, A coherent spin-photon interface in silicon, *Nature* **555**, 599 (2018).

[82] A. J. Landig, J. V. Koski, P. Scarlino, U. C. Mendes, A. Blais, C. Reichl, W. Wegscheider, A. Wallraff, K. Ensslin, and T. Ihn, Coherent spin-photon coupling using a resonant exchange qubit, *Nature* **560**, 179 (2018).

[83] C. X. Yu, S. Zihlmann, J. C. Abadillo-Uriel, V. P. Michal, N. Rambal, H. Niebojewski, T. Bedecarrats, M. Vinet, É. Dumur, M. Filippone, B. Bertrand, S. De Franceschi, Y.-M. Niquet, and R. Maurand, Strong coupling between a photon and a hole spin in silicon, *Nature Nanotechnology* **18**, 741 (2023).

[84] L. P. Kouwenhoven, S. Jauhar, J. Orenstein, P. L. McEuen, Y. Nagamune, J. Motohisa, and H. Sakaki, Observation of photon-assisted tunneling through a quantum dot, *Phys. Rev. Lett.* **73**, 3443 (1994).

[85] T. H. Oosterkamp, T. Fujisawa, W. G. van der Wiel, K. Ishibashi, R. V. Hijman, S. Tarucha, and L. P. Kouwenhoven, Microwave spectroscopy of a quantum-dot molecule, *Nature* **395**, 873 (1998).

[86] S. Gustavsson, M. Studer, R. Leturcq, T. Ihn, K. Ensslin, D. C. Driscoll, and A. C. Gossard, Frequency-selective single-photon detection using a double quantum dot, *Phys. Rev. Lett.* **99**, 206804 (2007).

[87] R. Leturcq, S. Gustavsson, M. Studer, T. Ihn, K. En

sslin, D. Driscoll, and A. Gossard, Frequency-selective single-photon detection with a double quantum dot, *Physica E: Low-dimensional Systems and Nanostructures* **40**, 1844 (2008).

[88] C. H. Wong and M. G. Vavilov, Quantum efficiency of a single microwave photon detector based on a semiconductor double quantum dot, *Phys. Rev. A* **95**, 012325 (2017).

[89] A. Gherri, S. Cornia, and M. Affronte, Microwave photon detectors based on semiconducting double quantum dots, *Sensors* **20**, 4010 (2020).

[90] W. Khan, P. P. Potts, S. Lehmann, C. Thelander, K. Dick, P. Samuelsson, and V. F. Maisi, Efficient and continuous microwave photoconversion in hybrid cavity-semiconductor nanowire double quantum dot diodes, *Nat. Comm.* **12**, 5130 (2021).

[91] S. Cornia, V. Demontis, V. Zannier, L. Sorba, A. Gherri, F. Rossella, and M. Affronte, Calibration-free and high-sensitivity microwave detectors based on InAs/InP nanowire double quantum dots, *Adv. Funct. Mater.* **33**, 2212517 (2023).

[92] S. Haldar, H. Havar, W. Khan, S. Lehmann, C. Thelander, K. A. Dick, and V. F. Maisi, Energetics of microwaves probed by double quantum dot absorption, *Phys. Rev. Lett.* **130**, 087003 (2023).

[93] S. Haldar, H. Havar, W. Khan, D. Zenelaj, P. P. Potts, S. Lehmann, K. A. Dick, P. Samuelsson, and V. F. Maisi, High-efficiency microwave photodetection by cavity-coupled double quantum dots with single-cavity-photon sensitivity, *Phys. Rev. Appl.* **24**, 044074 (2025).

[94] S. Haldar, D. Zenelaj, P. P. Potts, H. Havar, S. Lehmann, K. A. Dick, P. Samuelsson, and V. F. Maisi, Microwave power harvesting using resonator-coupled double quantum dot photodiode, *Phys. Rev. B* **109**, L081403 (2024).

[95] F. Oppliger, W. Jang, A. Tarascio, F. D. Palma, C. Reichl, W. Wegscheider, V. F. Maisi, D. Zumbühl, and P. Scarlino, High-efficiency tunable microwave photon detector based on a semiconductor double quantum dot coupled to a superconducting high-impedance cavity (2025), arXiv:2506.19828.

[96] J. M. Elzerman, R. Hanson, J. S. Greidanus, L. H. Willems van Beveren, S. De Franceschi, L. M. K. Vandersypen, S. Tarucha, and L. P. Kouwenhoven, Few-electron quantum dot circuit with integrated charge read out, *Phys. Rev. B* **67**, 161308 (2003).

[97] S. Haldar, D. Barker, H. Havar, A. Ranni, S. Lehmann, K. A. Dick, and V. F. Maisi, Continuous microwave photon counting by semiconductor-superconductor hybrids, *Phys. Rev. Lett.* **133**, 217001 (2024).

[98] D. Zueco, G. M. Reuther, S. Kohler, and P. Hänggi, Qubit-oscillator dynamics in the dispersive regime: Analytical theory beyond the rotating-wave approximation, *Phys. Rev. A* **80**, 033846 (2009).

[99] G. Zhu, S. Schmidt, and J. Koch, Dispersive regime of the Jaynes-Cummings and Rabi lattice, *New J. Phys.* **15**, 115002 (2013).

[100] C. Müller, Dissipative rabi model in the dispersive regime, *Phys. Rev. Res.* **2**, 033046 (2020).

[101] H.-P. Breuer and F. Petruccione, *The Theory of Open Quantum Systems* (Oxford University Press, Oxford, 2002).

[102] H. J. Carmichael, Quantum trajectory theory for cascaded open systems, *Phys. Rev. Lett.* **70**, 2273 (1993).

[103] C. W. Gardiner, Driving a quantum system with the output field from another driven quantum system, *Phys. Rev. Lett.* **70**, 2269 (1993).

[104] M. Field, C. G. Smith, M. Pepper, D. A. Ritchie, J. E. F. Frost, G. A. C. Jones, and D. G. Hasko, Measurements of Coulomb blockade with a noninvasive voltage probe, *Phys. Rev. Lett.* **70**, 1311 (1993).

[105] E. Buks, R. Schuster, M. Heiblum, D. Mahalu, and V. Umansky, Dephasing in electron interference by a ‘which-path’ detector, *Nature* **391**, 871 (1998).

[106] D. Sprinzak, Y. Ji, M. Heiblum, D. Mahalu, and H. Shtrikman, Charge distribution in a Kondo-correlated quantum dot, *Phys. Rev. Lett.* **88**, 176805 (2002).

[107] R. Schoelkopf, P. Wahlgren, A. Kozhevnikov, P. Delsing, and D. Prober, The radio-frequency single-electron transistor (RF-SET): A fast and ultrasensitive electrometer, *Science* **280**, 1238 (1998).

[108] D. J. Reilly, C. M. Marcus, M. P. Hanson, and A. C. Gossard, Fast single-charge sensing with a rf quantum point contact, *Appl. Phys. Lett.* **91**, 162101 (2007).

[109] C. Barthel, M. Kjærgaard, J. Medford, M. Stopa, C. M. Marcus, M. P. Hanson, and A. C. Gossard, Fast sensing of double-dot charge arrangement and spin state with a radio-frequency sensor quantum dot, *Phys. Rev. B* **81**, 161308 (2010).

[110] F. Vigneau, F. Fedele, A. Chatterjee, D. Reilly, F. Kuemmeth, M. F. Gonzalez-Zalba, E. Laird, and N. Ares, Probing quantum devices with radio-frequency reflectometry, *Appl. Phys. Rev.* **10**, 021305 (2023).

[111] J. I. Colless, A. C. Mahoney, J. M. Hornibrook, A. C. Doherty, H. Lu, A. C. Gossard, and D. J. Reilly, Dispersive readout of a few-electron double quantum dot with fast rf gate sensors, *Phys. Rev. Lett.* **110**, 046805 (2013).

[112] J. Z. Blumoff, A. S. Pan, T. E. Keating, R. W. Andrews, D. W. Barnes, T. L. Brecht, E. T. Croke, L. E. Euliss, J. A. Fast, C. A. Jackson, A. M. Jones, J. Kerckhoff, R. K. Lanza, K. Raach, B. J. Thomas, R. Velunta, A. J. Weinstein, T. D. Ladd, K. Eng, M. G. Borselli, A. T. Hunter, and M. T. Rakher, Fast and high-fidelity state preparation and measurement in triple-quantum-dot spin qubits, *PRX Quantum* **3**, 010352 (2022).

[113] H. Geng, M. Kiczynski, A. Timofeev, E. Osika, D. Keith, J. Rowlands, L. Kranz, R. Rahman, Y. Chung, J. Keizer, S. Gorman, and M. Y. Simmons, High-fidelity sub-microsecond single-shot electron spin readout above 3.5 k, *Nat. Commun.* **16**, 3382 (2025).

[114] G. Zheng, N. Samkharadze, M. L. Noordam, N. Kalhor, D. Brousse, A. Sammak, G. Scappucci, and L. M. Vandersypen, Rapid gate-based spin read-out in silicon using an on-chip resonator, *Nature Nanotechnology* **14**, 742 (2019).

[115] T. H. Swift, F. Olivier, G. Aizpurua-Iraola, J. Kirkman, G. M. Noah, M. de Kruif, F.-E. von Horstig, A. Gomez-Saiz, J. J. Morton, and M. F. Gonzalez-Zalba, A superinductor in a deep sub-micron integrated circuit (2025), arXiv:2507.13202.

[116] P. Scarlino, J. H. Ungerer, D. J. van Woerkom, M. Mancini, P. Stano, C. Müller, A. J. Landig, J. V. Koski, C. Reichl, W. Wegscheider, T. Ihn, K. Ensslin, and A. Wallraff, In situ tuning of the electric-dipole strength of a double-dot charge qubit: Charge-noise

protection and ultrastrong coupling, *Phys. Rev. X* **12**, 031004 (2022).

[117] P. Harvey-Collard, G. Zheng, J. Dijkema, N. Samkharadze, A. Sammak, G. Scappucci, and L. M. K. Vandersypen, On-chip microwave filters for high-impedance resonators with gate-defined quantum dots, *Phys. Rev. Appl.* **14**, 034025 (2020).

[118] N. Holman, D. Rosenberg, D. Yost, J. Yoder, R. Das, W. D. Oliver, R. McDermott, and M. Eriksson, 3D integration and measurement of a semiconductor double quantum dot with a high-impedance TiN resonator, *npj Quantum Inf.* **7**, 137 (2021).

[119] N. Holman, J. Dodson, L. Edge, S. Coppersmith, M. Friesen, R. McDermott, and M. Eriksson, Microwave engineering for semiconductor quantum dots in a cQED architecture, *Appl. Phys. Lett.* **117** (2020).

[120] J. Xia, E. Adams, V. Shvarts, W. Pan, H. Stormer, and D. Tsui, Ultra-low-temperature cooling of two-dimensional electron gas, *Physica B: Condensed Matter* **280**, 491 (2000).

[121] N. Samkharadze, A. Kumar, M. J. Manfra, L. Pfeiffer, K. West, and G. Csáthy, Integrated electronic transport and thermometry at millikelvin temperatures and in strong magnetic fields, *Rev. Sci. Instrum.* **82**, 053902 (2011).

[122] Z. Iftikhar, A. Anthore, S. Jezouin, F. D. Parmentier, Y. Jin, A. Cavanna, A. Ouerghi, U. Gennser, and F. Pierre, Primary thermometry triad at 6 mK in mesoscopic circuits, *Nat. Commun.* **7**, 12908 (2016).

[123] G. Nicolí, P. Märki, B. A. Bräm, M. P. Röösli, S. Hennel, A. Hofmann, C. Reichl, W. Wegscheider, T. Ihn, and K. Ensslin, Quantum dot thermometry at ultra-low temperature in a dilution refrigerator with a 4He immersion cell, *Rev. Sci. Instrum.* **90**, 113901 (2019).

[124] A. Jones, C. Scheller, J. Prance, Y. Kalyoncu, D. Zumbühl, and R. Haley, Progress in cooling nanoelectronic devices to ultra-low temperatures, *J. Low Temp. Phys.* **201**, 772 (2020).

[125] L. Camenzind, S. Geyer, A. Fuhrer, R. Warburton, D. Zumbühl, and A. Kuhlmann, A hole spin qubit in a fin field-effect transistor above 4 kelvin, *Nature Electronics* **5**, 178 (2022).

[126] M. Sarsby, N. Yurtagül, and A. Geresdi, 500 microkelvin nanoelectronics, *Nat. Commun.* **11**, 1492 (2020).

[127] L. V. Levitin, H. van der Vliet, T. Theisen, S. Dimitriadi, M. Lucas, A. D. Corcoles, J. Nyéki, A. J. Casey, G. Creeth, I. Farrer, D. A. Ritchie, J. Nicholls, and J. Saunders, Cooling low-dimensional electron systems into the microkelvin regime, *Nat. Commun.* **13**, 667 (2022).

[128] S. Matern, K. Macieszczak, S. Wozny, and M. Leijnse, Metastability and quantum coherence assisted sensing in interacting parallel quantum dots, *Phys. Rev. B* **107**, 125424 (2023).

[129] J. Y. Huang, R. Y. Su, W. H. Lim, M. Feng, B. Van Straaten, B. Severin, W. Gilbert, N. Dumoulin Stuyck, T. Tanttu, S. Serrano, *et al.*, High-fidelity spin qubit operation and algorithmic initialization above 1 K, *Nature* **627**, 772 (2024).

[130] G. T. Landi, M. J. Kewming, M. T. Mitchison, and P. P. Potts, Current fluctuations in open quantum systems: Bridging the gap between quantum continuous measurements and full counting statistics, *PRX Quantum* **5**, 020201 (2024).